UNIVERSITAT POLITÈCNICA
DE
CATALUNYA

ESCOLA SUPERIOR D'ENGINYERIES INDUSTRIAL,
AEROESPACIAL I AUDIOVISUAL DE TERRASSA

Computational Fluid Dynamics: Fractional Step Method and its applications in internal and external flows

Degree in Aerospace Technology Engineering

Student: Montllor Ramoneda, Marcel
Director: Oliva Llena, Asensio
Co-Director: Pérez Segarra, Carles-David

Delivery date: June, 10th 2018

Contents

Page

List of Figures

List of Tables

1 Introduction

1.1 Aim

The aim of this project is to solve problems mainly related to Fluid Dynamics through the 'Fractional Step Method'. This method is based on the Helmholtz-Hodge theorem, which is explained in this thesis, and it is only useful when the flow is incompresible. However, before start talking about this method and its applications, a pure diffusion and a convection-diffusion cases are solved in order to check the validity of the codes used.

These codes are developed in C++ language, although the data obtained is treated with MatLab.

1.2 Requirements

The requirements for this thesis are the development of C++ codes, enabling to solve the different equations and problems exposed. It is also necessary to develop MatLab codes in order to visualize the data obtained with C++ codes.

Turbulent flows are not treated in this study since they require methodologies such complex that could be the main aim of another thesis.

1.3 State of the art and justification

Most of engineering fields have a lot of difficult problems which can be modeled with complex differential equations. These equations can not always be explained analytically, so it is necessary to implement numerical methods to find approximated solutions. Numerical calculus appears as a useful tool to understand and simulate real cases which time ago were impossible to do.

The number of techniques used in numerical methods has increased these last years. The power of the computers is also increasing, enabling the continuous development of the codes and the possibility of increasing their accuracy.

Numerical analysis has become very important in aerospace and automotive industry. This kind of technology can avoid several tests, since it can predict the performance of some devices which would be very expensive to build a prototype and prove it. In this way, Computational Fluid Dynamics prevent to waste this huge amount of money. It lets to optimize the model before you build it, in order to get the best tests performances without spending unnecessary money.

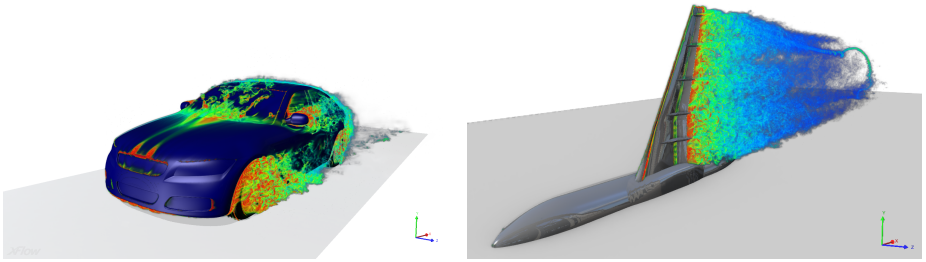

(a) (b)

Figure 1: Examples of computational fluid dynamic applications[1]

These reasons explained justify the study of computational fluid dynamics, in order to understand and apply physical and mathematical concepts that allow to simulate real cases.

1.4 Scope

The project starts with an explanation of the basic equations needed to study the fluid dynamics. A basic problem with a known solution is presented in order to explain the pure diffusion case. Then are shown the typical schemes used to solve the convection-diffusion equation, which has an important role in fluid dynamics.

Once it is done, 'Fractional Step Method'(FSM) is explained, an explicit method which enables to solve the Navier-Stokes equations with incompressible flow. It is also shown the structure of the code developed to use the method mentioned. Then, there is a section which verifies the code and analyse the solutions obtained comparing with a known case called 'Lid-Driven Cavity'.

The last part treats with the performance of a laminar flow between two flat plates. Checking this enables to simulate solid geometries between the plates, as if it were a wind tunnel at low Reynolds number. However, as it has been said, the methodology used does not allow the script to simulate turbulent flows.

Finally are shown some conclusions about the thesis.

2 Mathematical formulation. Numerical resolution of the generic convection-diffusion equation

2.1 Introduction

This section shows the basic formulation of the Navier-Stokes equations and their meaning. Then are solved the cases of pure diffusion and convection-diffusion applied to specific problems whose solutions are known.

For the case of pure diffusion the problem is related to heat transfer, and it consists of a long rod with a square cross section composed of 4 different materials and 4 different boundary conditions.

The case of convection-diffusion is checked with 4 different problems. There are 2 of them that can be solved analytically, and it makes easier to compare the accuracy of the solution. The other 2 problems are typically used to validate the convection-diffusion, and their solutions are extracted from literature.

2.2 Navier-Stokes formulation

The Navier Stokes equations describes the motion of a fluid. In order to do that, they show the relations between velocity, pressure, temperature and density of a fluid [2]. These equations were developed in the early 1800's. In fact, they were an extension of the Euler equations, but considering the viscosity on the flow.

Navier-Stokes equations have never been solved analytically. They are one of the 'Millennium problems' defined by 'The Clay Mathematics Institute'[3]. 'Millenium problems' are 7 selected problems focused on important classic questions that have resisted solution over the years. However, there are some approximations and simplifications which make Navier-Stokes equations less complex.

The Navier-Stokes equations are 3: mass, momentum and energy. The following development is extracted from [4].

1. Mass conservation equation: This equation describes the conservation of the mass.

$$\frac{D}{Dt}\int_{V_m(t)} \rho dV = 0 \tag{1a}$$

Through the Reynolds transport theorem, this equation yields to:

$$\frac{\partial}{\partial t}\int_{CV} \rho dV + \int_{CS} \rho \vec{v}\cdot\vec{n}dS = 0 \tag{1b}$$

The first integral of equation 1b refers to the variation of the density along the time inside a defined volume, and the second integral represents the mass flow which pass through the surfaces of this volume. If it is considered a differential volume dV, equation 1c is achieved.

$$\frac{\partial(\rho dV)}{\partial t} - \dot{m}_x + \dot{m}_{x+dx} - \dot{m}_y + \dot{m}_{y+dy} - \dot{m}_z + \dot{m}_{z+dz} = 0 \begin{cases} \dot{m}_x = \rho v_x dydz \ \ ... \\ \dot{m}_{x+dx} = \dot{m}_x + \frac{\partial \dot{m}_x}{\partial x}dx \ \ ... \end{cases} \tag{1c}$$

Then, working with the terms of equation 1c and dividing by dV:

$$\frac{\partial \rho}{\partial t} + \frac{\partial(\rho v_x)}{\partial x} + \frac{\partial(\rho v_y)}{\partial y} + \frac{\partial(\rho v_z)}{\partial z} \tag{1d}$$

Equation 1d can be expressed as equations 1e,1f and 1g.

$$\frac{\partial \rho}{\partial t} + \frac{\partial(\rho v_k)}{\partial x_k} = 0 \tag{1e}$$

$$\frac{\partial \rho}{\partial t} + \nabla\cdot(\rho\vec{v}) = 0 \tag{1f}$$

$$\frac{D\rho}{Dt} + \rho\nabla\cdot\vec{v} = 0 \tag{1g}$$

For incompressible flows (where $\rho = \rho_o$), the resultant equation is $\nabla\cdot\vec{v} = 0$.

2. Linear momentum equations: Describes the linear momentum conservation in a system. In fact, this is a deeper way of dealing with Newton's second law. This equation is splitted in 3 components, one for each direction. As it has been done with mass conservation, the first step is to use the Reynolds transport theorem (equation 2a to 2b):

$$\frac{D}{Dt}\int_{V_m(t)} \vec{v}\rho dV = 0 \tag{2a}$$

$$\frac{\partial}{\partial t}\int_{CV} \vec{v}\rho dV + \int_{CS} \vec{v}\rho\vec{v}\cdot\vec{n}dS = \int_{CS} \vec{f_{\vec{n}}}dS + \int_{CV} \vec{f_b}dV \tag{2b}$$

Where $\vec{f_n}$ represents the surfaces forces (pressure and viscosity), while $\vec{f_b}$ represents the body forces (mass and electromagnetic). If these forces are developed mathematically, equation 2c is got.

$$\frac{\partial}{\partial t}\int_{CV} \vec{v}\rho dV + \int_{CS} \vec{v}\rho\vec{v}\cdot\vec{n}dS = -\int_{CS} p\vec{n}dS + \int_{CS} \vec{n}\cdot\vec{\tau}dS + \int_{CV} \vec{g}\rho dV + \int_{CV} \vec{f^e}dV \tag{2c}$$

Working with equation 2c in 'x' direction and considering a volume dV, equation 2d is obtained.

$$\begin{aligned} &\frac{\partial(v_x\rho dV)}{\partial t} - (\dot{m}v_x)_x + (\dot{m}v_x)_{x+dx} - (\dot{m}v_x)_y + (\dot{m}v_x)_{y+dy} - (\dot{m}v_x)_z + (\dot{m}v_x)_{z+dz} \\ &= (p)_x dydz - (p)_{x+dx}dydz - (\tau_{xx})_x dydz + (\tau_{xx})_{x+dx}dydz - (\tau_{yx})_y dxdz \\ &\quad + (\tau_{yx})_{y+dy}dxdz - (\tau_{zx})_z dxdy + (\tau_{zx})_{z+dz}dxdy + \rho g_x dV + f_x^e dV \end{aligned} \tag{2d}$$

Then, developing the terms of equation 2d, it yields to equation 2e (see development similarities with equation 1c and 1d).

$$\begin{aligned}&\frac{\partial(\rho v_x)}{\partial t}dV+\frac{\partial(\dot{m}v_x)_x}{\partial x}dx+\frac{\partial(\dot{m}v_x)_y}{\partial y}dy+\frac{\partial(\dot{m}v_x)_z}{\partial z}dz\\&=-\frac{\partial p}{\partial x}dV+\frac{\partial\tau_{xx}}{\partial x}dV+\frac{\partial\tau_{yx}}{\partial y}dV+\frac{\partial\tau_{zx}}{\partial z}dV+\rho g_x dV+f_x^e dV\end{aligned}\tag{2e}$$

If equation 2e is divided by dV, equations 2f, 2g and 2h are achieved (each one represents one direction of momentum).

$$\frac{\partial(\rho v_x)}{\partial t}+\frac{\partial(\rho v_x v_x)}{\partial x}+\frac{\partial(\rho v_y v_x)}{\partial y}+\frac{\partial(\rho v_z v_x)}{\partial z}=-\frac{\partial p}{\partial x}+\frac{\partial\tau_{xx}}{\partial x}+\frac{\partial\tau_{yx}}{\partial y}+\frac{\partial\tau_{zx}}{\partial z}+\rho g_x+f_x^e\tag{2f}$$

$$\frac{\partial(\rho v_y)}{\partial t}+\frac{\partial(\rho v_x v_y)}{\partial x}+\frac{\partial(\rho v_y v_y)}{\partial y}+\frac{\partial(\rho v_z v_y)}{\partial z}=-\frac{\partial p}{\partial y}+\frac{\partial\tau_{xy}}{\partial x}+\frac{\partial\tau_{yy}}{\partial y}+\frac{\partial\tau_{zy}}{\partial z}+\rho g_y+f_y^e\tag{2g}$$

$$\frac{\partial(\rho v_z)}{\partial t}+\frac{\partial(\rho v_x v_z)}{\partial x}+\frac{\partial(\rho v_y v_z)}{\partial y}+\frac{\partial(\rho v_z v_z)}{\partial z}=-\frac{\partial p}{\partial z}+\frac{\partial\tau_{xz}}{\partial x}+\frac{\partial\tau_{yz}}{\partial y}+\frac{\partial\tau_{zz}}{\partial z}+\rho g_z+f_z^e\tag{2h}$$

$$\frac{\partial(\rho\vec{v})}{\partial t}+\nabla\cdot(\rho\vec{v}\vec{v})=-\nabla p+\nabla\cdot\vec{\tau}+\rho\vec{g}+\vec{f^e}\tag{2i}$$

Using the mass conservation, it is possible to demonstrate that:

$$\frac{\partial(\rho\vec{v})}{\partial t}+\nabla\cdot(\rho\vec{v}\vec{v})=\rho\frac{\partial\vec{v}}{\partial t}+\rho(\vec{v}\cdot\nabla)\vec{v}=\rho\frac{D\vec{v}}{Dt}\tag{2j}$$

The tensor $\vec{\tau}$ for Newtonian fluids is:

$$\vec{\tau}=\mu(\nabla\vec{v}+\nabla\vec{v}^T)-\frac{2}{3}\mu(\nabla\cdot\vec{v})\vec{\delta}\tag{2k}$$

If it is considered that the properties are constant, the resultant equation is:

$$\rho_o\frac{\partial\vec{v}}{\partial t}+\rho_o\nabla\cdot(\vec{v}\vec{v})=-\nabla p+\mu_o\nabla^2\vec{v}+\rho_o\vec{g}+\vec{f^e}\tag{2l}$$

3. Total and thermal energy equations: These equations are not used to solve the problems proposed to study with 'Fractional Step Method'. However, it is shown the basic formulation since the pure diffusion case is related to the thermal equation.
Before talk about the total energy equation, it is useful to show the kinetic energy equation 3a.

$$\rho\frac{De_c}{Dt}=-\nabla\cdot(\rho\vec{v})+p\nabla\cdot\vec{v}+\nabla\cdot(\vec{v}\cdot\vec{\tau})-\vec{\tau}:\nabla\vec{v}+\rho\vec{v}\vec{g}+\vec{v}\cdot\vec{f^e}\tag{3a}$$

$$\text{Plank's postulate}\qquad\vec{\tau}:\nabla\vec{v}\geqslant 0\tag{3b}$$

Plank's postulate says that the dissipation due to viscosity is always positive ($\vec{\tau}:\nabla\vec{v}\geqslant 0$).
Then, the total energy can be written as equation 3c, and it is yielded to equation 3d through the Reynolds transport theorem.

$$\frac{D}{Dt}\int_{V_m(t)}e\rho dV=0\tag{3c}$$

$$\frac{\partial}{\partial t}\int_{CV}e\rho dV+\int_{CS}e\rho\vec{v}\cdot\vec{n}dS=-\int_{CS}\vec{q}\cdot\vec{n}dS+\int_{CS}\vec{v}\cdot\vec{f}_{\vec{n}}dS+\int_{CV}\vec{v}\cdot\vec{g}\rho dV+\int_{CV}\vec{E}\cdot\vec{j}dU\tag{3d}$$

Analysing and developing term by term of equation 3d in a differential control volume, and dividing by dV, equation 3e is achieved.

$$\frac{\partial(\rho e)}{\partial t} + \nabla \cdot (\rho \vec{v} e) = -\nabla \cdot \vec{q} - \nabla \cdot (p\vec{v}) + \nabla \cdot (\vec{v} \cdot \vec{\tau}) + \rho \vec{v} \cdot \vec{g} + \vec{E} \cdot \vec{j} \tag{3e}$$

Working with the fact that the energy is the sum of kinetic and potential energy, and using equation 3a:

$$\rho \frac{Du}{Dt} = -\nabla \cdot \vec{q} - p\nabla \cdot \vec{v} + \vec{\tau} : \nabla \vec{v} + \Phi^e \quad where \rightarrow \Phi^e = \frac{\vec{j}\vec{j}}{\sigma_e} \tag{3f}$$

It is important to distinct between equation 3e and equation 3f. The first one refers to the total energy of the fluid, while the second one is the thermal energy. The term $\vec{q}$ stands for conduction and radiation. Taking the following assumptions:

- Semi-perfect gas ($du = C_v dT$, $C_v(T)$), and no radiation.
- Incompressible flows($\rho = \rho_o$, $\nabla \cdot \vec{v} = 0$, $du = C_p dT$, $C_p(T)$).
- Negligible viscous dissipation and $\Phi^e = 0$

The thermal equation can be written as:

$$\rho_o C_p (\frac{\partial T}{\partial t} + \vec{v} \cdot \nabla T) = \nabla \cdot (\lambda \nabla T) \tag{3g}$$

2.3 Heat Transfer problem - Pure diffusion

As it has been said in section 1, a pure diffusion problem whose solution is known is solved. This problem is related to heat transfer, and it is necessary to use the thermal equation 3g considering that the system is solid ($\vec{v} = 0$). It is possible to see that there is only diffusion in this case. The equation yields to 4a, which can be rewritten as 4b through the divergence theorem.

$$\int_{CV} \rho_o C_p \frac{\partial T}{\partial t} dV = \int_{CV} \nabla \cdot (\lambda \nabla T) dV \tag{4a}$$

$$\int_{CV} \rho_o C_p \frac{\partial T}{\partial t} = \int_{CS} \lambda \nabla T \vec{n} dS \tag{4b}$$

The problem, extracted from document [5], consists in a long rod composed of four different materials (see figure 2). With the boundary conditions given in table 3, the heat conduction equation has to be solved in order to achieve the temperatures map for each time steep during the first 10,000 seconds. It implies to choose a suitable mesh which allows a good precision in front the time step and the geometry of the problem.

The points coordinates are shown in table 1, and the material properties are given in table 2.

	x(m)	y(m)
p_1	0.50	0.40
p_2	0.50	0.70
p_3	1.10	0.80

Table 1: Heat transfer problem coordinates [5]

Once the problem is solved, temperature at locations (0.65,0.56) and (0.74,0.72) are shown second by second during the first 10,000 seconds in order to observe the time evolution at these points.

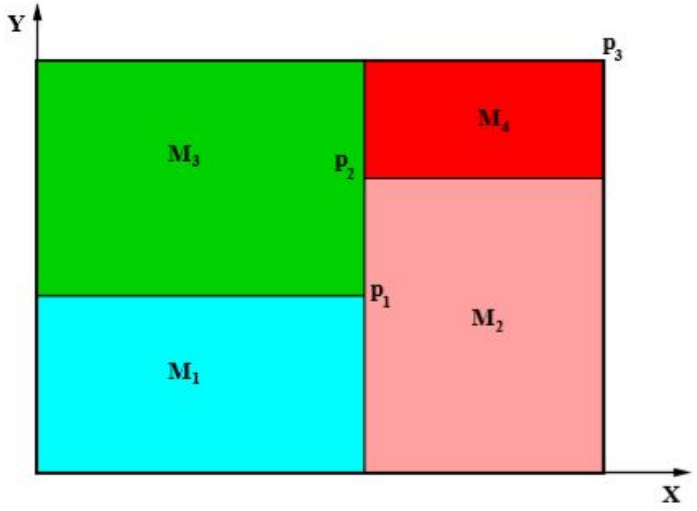

Figure 2: General schema heat transfer problem [5]

	$\rho\,[kg/m^3]$	$C_p\,[J/kgK]$	$k\,[W/mK]$
M_1	1,500.00	750.00	170.00
M_2	1,600.00	770.00	140.00
M_3	1,900.00	810.00	200.00
M_4	2,500.00	930.00	140.00

Table 2: Physical properties heat transfer problem [5]

Cavity wall	Boundary condition
Bottom	Isotherm at T=23.00°C
Top	Uniform $Q_{flow} = 60.00W/m$ length
Left	In contact with a fluid at $T_g = 33.00°C$ and heat transfer coefficient $9.00W/m^2K$
Right	Uniform temperature T=8.00+0.005t°C (where t is the time in seconds)

Table 3: Boundary conditions heat transfer problem [5]

2.3.1 Equations problem heat transfer

The problem is solved with the central nodes method, which is represented in figure 3.

At any node inside the geometry, the main equation has structure of equation 5, which is the result of discretizing equation 4b[6].

$$a_P T_P^{n+1} = a_E T_E^{n+1} + a_W T_W^{n+1} + a_N T_N^{n+1} + a_S T_S^{n+1} + b_P \tag{5}$$

These coefficients are calculated as:

$$a_{N,S,E,W} = \beta \lambda_{N,S,E,W}^{n+1} \frac{S_{n,s,e,w}}{d_{P-N,S,E,W}} \tag{6}$$

$$a_P = a_E + a_W + a_N + a_S + \frac{\rho_P V_P C_P}{\Delta t} \tag{7}$$

$$b_P = \beta q_{vP}^{n+1} + (1-\beta)\dot{Q}_P^n + \frac{\rho_P V_P C_P T_P^n}{\Delta t} \tag{8}$$

- The subscripts N,S,E,W refers to the relative positions of the nodes: north, south, east or west.
- The superscripts n and n+1 refers to the relative time of the variable.
- V, S and d refers to the volume of the control volume, area between two control volumes and distance between two nodes.
- β is the parameter used to define the type of integration used.
  - If $\beta = 1$ the integration is implicit.
  - If $\beta = 0$ the integration is explicit.
  - If $\beta = 0.5$ the integration is with the Crank Nicolson method.
- The parameters ρ, C_P and λ refers to the material properties (density, capacity and conductivity).
- $\dot{Q}_P^n$ is the heat conduced at the previous time.

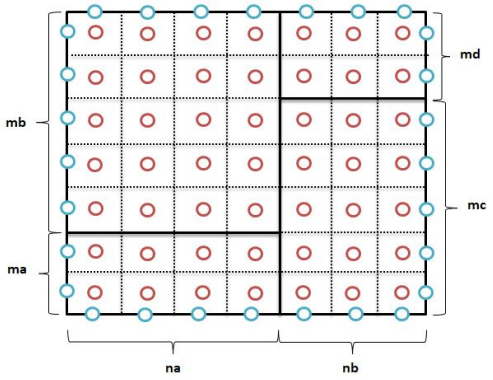

Figure 3: Central nodes method

This equation has to be solved at each node considering the material properties, which depends on the location of this node. The geometry mentioned at any control volume is shown in figure 4.

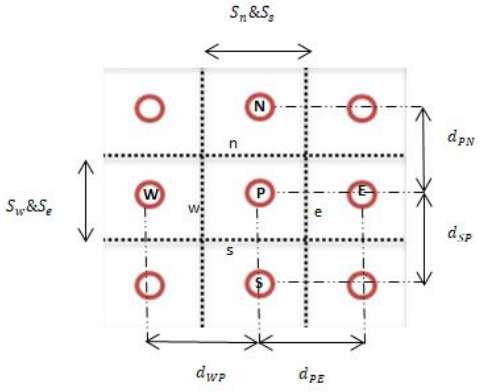

Figure 4: Geometry control volume

As it can be seen in figure 3, the changes of the materials coincide with the cell faces of the control volumes. It must be considered when λ is calculated:

$$\lambda_x = \frac{d_{PX}}{\frac{d_{Px}}{\lambda_P} + \frac{d_{xX}}{\lambda_X}} \tag{9}$$

Where 'x' refers to the position of the wall considered (n,s,e,w) and 'X' refers to the position of the node (N,S,E,W).

2.3.2 Boundary conditions

The equations are different at the boundary nodes, due to the conditions shown in table 3. On bottom and right walls, the temperatures are directly imposed (the first one is constant and the second one depends on the time). On the left wall, the heat transfer coming from the west is because of the convection. Then, it is possible to get the temperature of the node through the heat equilibrium (see figure 5).

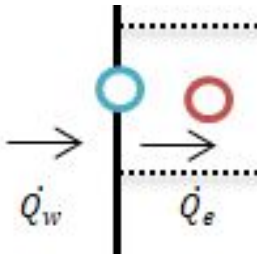

Figure 5: Left boundary conditions

It yields to the equation 10:

$$\alpha(T_g - T_P^{n+1}) = -\lambda_e \frac{T_E^{n+1} - T_P^{n+1}}{d_{PE}} \tag{10}$$

Where α is the heat transfer coefficient, and T_g the temperature of the fluid. From this equation it is possible to isolate the temperature of the boundary node.

The top wall has an uniform heat flow of $Q_{flow} = 60.00 W/m$. As it has been done before, to figure out the temperature of the node it is necessary to do a heat equilibrium.

$$-\lambda_s \frac{T_P^{n+1} - T_S^{n+1}}{d_{SP}} = -Q_{flow} \tag{11}$$

The flux on the wall (Q_{flow}) is in the opposite direction of the axis, so it must be considered negative in this equation.

The geometry of the control volumes on the walls is also different (see figure 3). The distance between the nodes is divided by 2. However, as the equilibrium is done only at the wall, it is not necessary to use the surface area since it is the same at each side.

2.3.3 Script Heat Transfer problem

The script scheme is shown in figure 6.

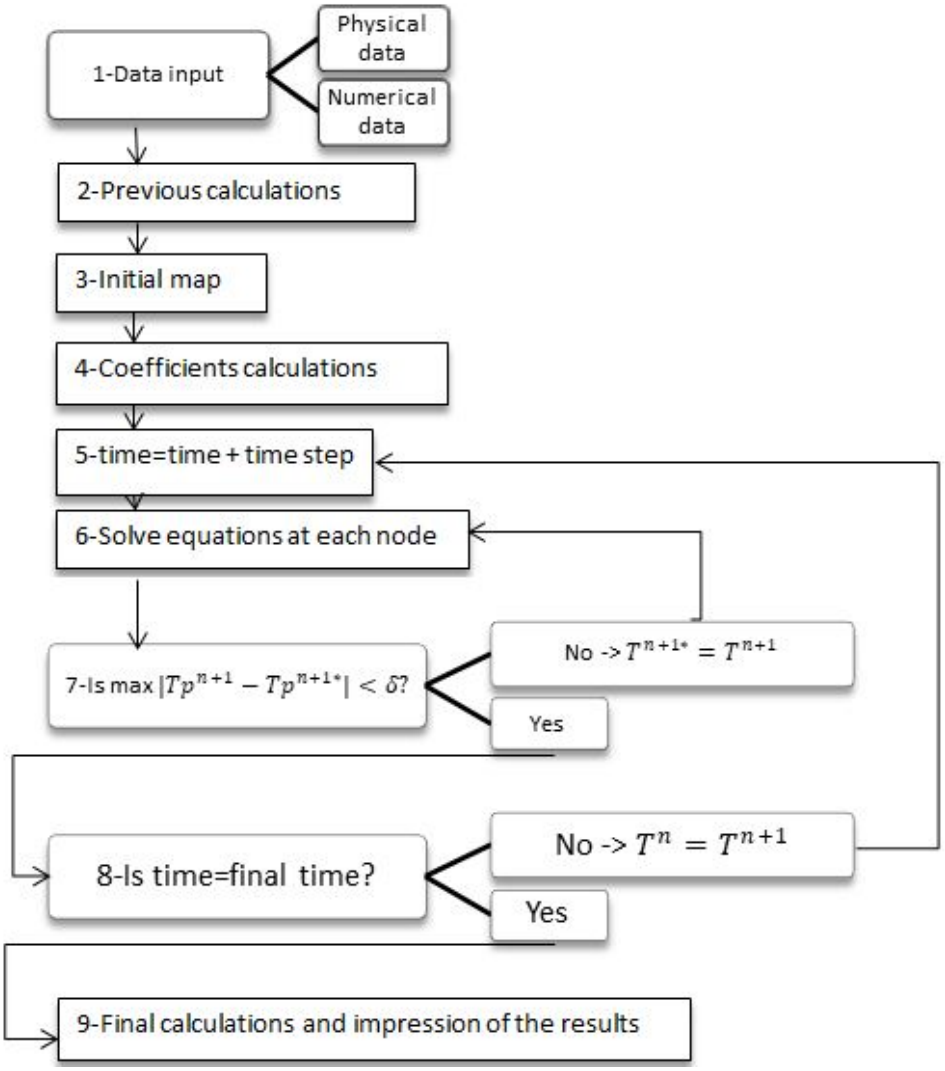

Figure 6: Scheme of the script

1. All data input
   - Physical data: geometry, material properties, boundary conditions, initial temperature...
   - Numerical data: convergence factor (δ), β, number of divisions, time discretization...
2. Previous calculations: compute the volumes, areas, distances...
3. Initial map: set the initial temperature at each node.
4. Coefficients calculations: save the value of the coefficients shown in equations 6 and 7 for each node .
5. Next time step.
6. Solve the equations shown in section 2.3.1 in order to figure out the temperature at each node.

7. Check the convergence of the solution founded.
   - If solution has not converged → go to step 6 with the new temperatures map.
   - If solution has converged → next step.
8. Is the actual time the last one?
   - No → go to step 5.
   - Yes → next step.
9. Final calculations and impression of the results.

2.3.3.1 Gauss-Seidel and TDMA line by line

This linear solver shown in the script is called 'Gauss-Seidel'. It solves the equation at each node and compares if the new solution has converged. Another typical linear solver which is better talking about the computational cost is 'line by line'. This kind of solver is used in other codes of the thesis, where efficiency gets more important. It solves the nodes line by line using the TDMA (Tridiagonal Matrix Algorithm)[7] and then column by column.

A tridiagonal system of equations is that composed by simultaneous algebraic equations with a nonzero coefficients only on the main diagonal, the lower diagonal and the upper diagonal.

$$\begin{bmatrix} a_{P_1} & -a_{E_1} & & & & & \\ -a_{W_2} & a_{P_2} & -a_{E_2} & & & & \\ & -a_{W_3} & a_{P_3} & -a_{E_3} & & & \\ & & & \dots & & & \\ & & & & \dots & & \\ & & & -a_{W_{n-1}} & a_{P_{n-1}} & -a_{E_{n-1}} & \\ & & & & -a_{W_n} & a_{P_n} & \end{bmatrix} \begin{bmatrix} T_1 \\ T_2 \\ T_3 \\ \dots \\ \dots \\ T_{n-1} \\ T_n \end{bmatrix} = \begin{bmatrix} b_1 \\ b_2 \\ b_3 \\ \dots \\ \dots \\ b_{n-1} \\ b_n \end{bmatrix} \tag{12}$$

TDMA is the result of applying a Gaussian elimination to the tridiagonal system of equations.

$$P_i = \frac{-a_{E_i}}{a_{P_i} + a_{W_i} P_{i-1}} \qquad Q_i = \frac{b_i - a_{W_i} Q_{i-1}}{a_{P_i} + a_{W_i} P_{i-1}} \tag{13}$$

The procedure consists in calculate the coefficients of equation 13 from the first node of a line to the last one. Then, when all these coefficients are calculated, it is possible to obtain directly the temperature at each node through equation 14, which has to be solved from the last node to the first one.

$$T_i = P_i T_{i+1} + Q_i \tag{14}$$

However, it is easy to see that this method is only applicable to a one-dimensional problem (where the only unknowns are west, est and main nodes for instance). 'Line by line' consists in solving each line through TDMA, then do the same with each column, and finally compare if the new solution has converged. If not, another iteration is necessary until it has converged. It is important to notice that the coefficients '$a_N T_N + a_S T_S$' are inside the coefficient 'b' when a line is solved, and the same happens with coefficients '$a_W T_W + a_E T_E$' when a column is solved.

It is easy to see that this method is more efficient than Gauss-Seidel, since it solves each line while Gauss-Seidel solves node by node.

2.3.4 Results Heat Transfer problem

2.3.4.1 Mesh study

The mesh geometry discretization is done in order to get the same position of the nodes in 'y' direction at both sides (left and right from p1 and p2, figure 2). For this reason, the number of divisions in this direction is imposed by the following rules (regarding to criteria in picture 3):

$$ma + mb = mc + md \tag{15}$$

$$\frac{p1_y}{ma} = \frac{p3_y - p1_y}{mb} = \frac{p2_y}{mc} = \frac{p3_y - p2_y}{md} \tag{16}$$

All the parameters of the equation 15 must be integrers. Equation 16 shows the relations between these divisions, using the coordinates shown in table 1:

$$ma = mb \qquad mc = 1.75ma \qquad md = 0.25ma \tag{17}$$

In order to achieve an integer number, 'ma' must be a multiple of 4.

This issue does not appear in 'x' direction, since there is no problem if the left side is disretized different from the right side.

For the reasons explained above, the mesh convergence in terms of geometry is studied with the minimum number of nodes in 'y' direction (ma=4) and changing the discretization in 'x' direction. The convergence of the temperature at node (0.74,0.72) is shown in figure 7. The time discretization is the same for all the cases shown.

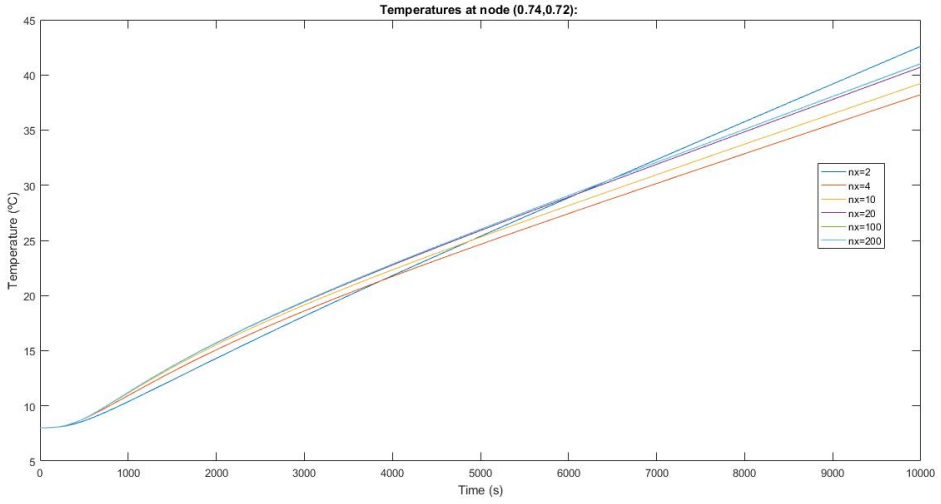

Figure 7: Temperatures at node (0.74,0.72) changing the value of 'nx'

The 'nx' of the legend refers to the sum of 'na' and 'nb' divisions, considering that na=nb. It is important to realize that the coordinates of the point depends on the discretization that has been done. Hence, if nx=2 the temperature shown in the graph 7 is the temperature of the nearest node to the coordinates (0.74,0.72). For this reason, the accuracy of the results will not be as good as it could. An improvement to this issue would be a discretization which were adapted in order to have a node in this exact point, or an interpolation between the nearest results.

Figure 8 shows the same than figure 7 but amplified.

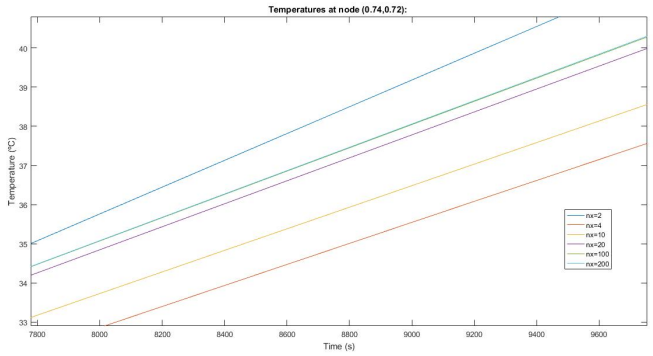

Figure 8: Temperatures at node (0.74,0.72) between 7,800s and 10,000s changing the value of 'nx'

The difference between nx=100 and nx=200 is low enough to consider that the solution has converged (in fact, both lines are superposed, so it is difficult to differentiate). The value used since now will be nx=100 in order to have the highest accuracy without increasing the computational cost. Once it is done, the next step is to check the convergence of the solution in 'y' direction. As it has been said, the divisions have to satisfy the rules of equation 17. Then, 'ma' must be a multiple of 4 to have all the other divisions as integers.

Since now, 'my' will be considered as the sum of ma+mb (which must be the same than mc+md). In figure 9 is shown the temperature at the determined node in front of the time, changing the 'y' axis disretization. It can be seen that the changes of the values of temperatures are small, so it is considered that the solution has converged when my=80 (see figure 9(b)). It is the value used for the next analyses.

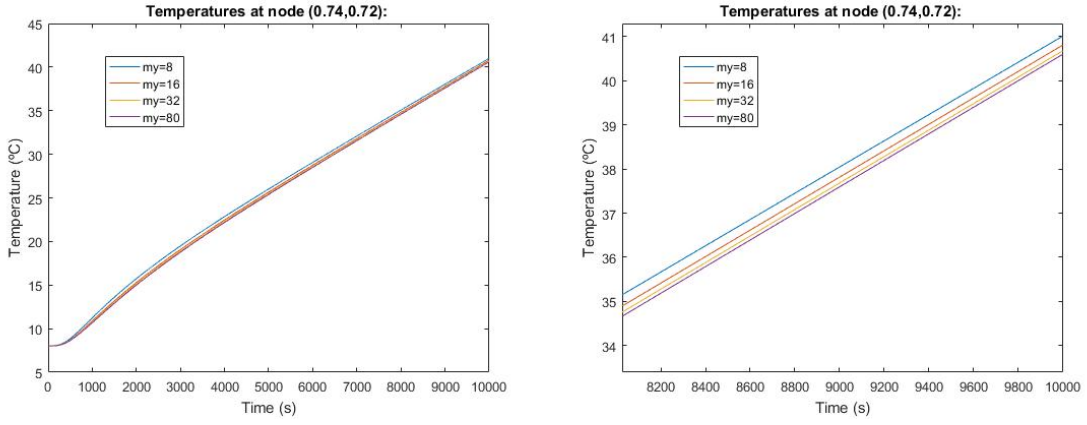

(a) Overview

(b) Amplified view

Figure 9: Temperatures at node (0.74,0.72) changing the value of 'my'

The last part of the mesh study consists in analyse the time discretization. The geometry of the mesh has been chosen before, and it is got the one which has converged with the minimum number of nodes, in order to reduce the computational cost.

In figure 10 are shown the temperatures at the node with coordinates (0.74,0.72) changing the time discretization. Table 4 shows the equivalent step time for each discretization. In figure 10(a) it is possible to see that increasing the number of time steps (reducing the time step value) the solution does not get converged completely. Obviously, the most accurate solution is the one with

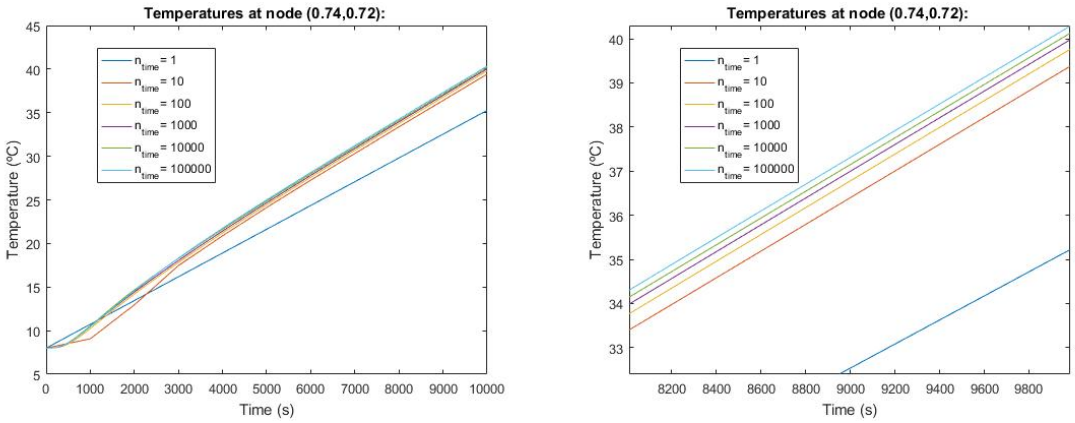

(a) Overview (b) Amplified view

Figure 10: Temperatures at node (0.74,0.72) changing the time discretization

more elements, but the time of execution with this mesh increases too much compared with the others (see figure 11). However, it must be evaluated the precision needed and chose the time discretization which fits with the requirements of the user.

n_{time}	$t_{step}(s)$
1	10,000
10	1,000
100	100
1,000	10
10,000	1
100,000	0.1

Table 4: Time step vs number of time divisions

Figure 11 shows the time of execution in front of the number of time divisions. It is important to notice that in figure 11(b) the 'x' axis is in logarithmic scale. It means that increasing 10 times the time discretization increases the time cost in an exponential way.

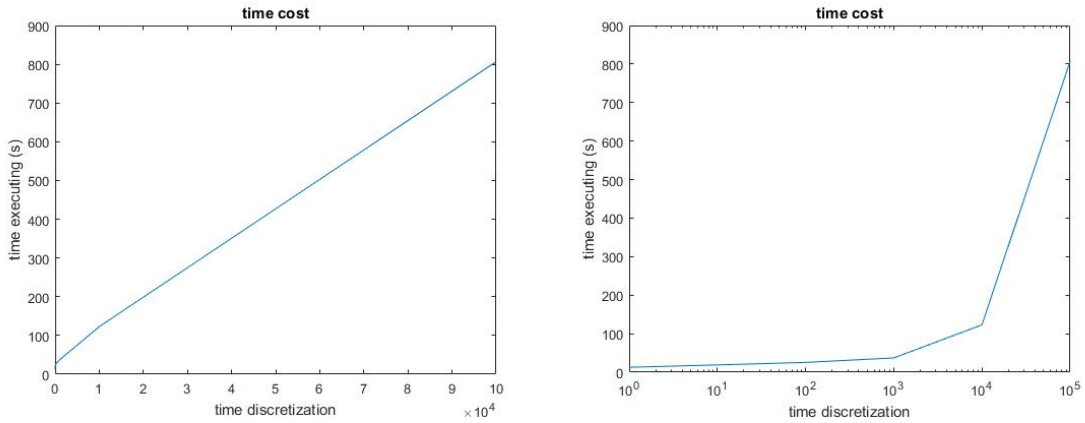

(a) Linear scale (b) Logarithmic scale

Figure 11: Time of execution vs number of time divisions

2.3.4.2 Final results Heat Transfer problem

The temperatures at points (0.74,0.72) and (0.65,0.56) are shown in figure 12.

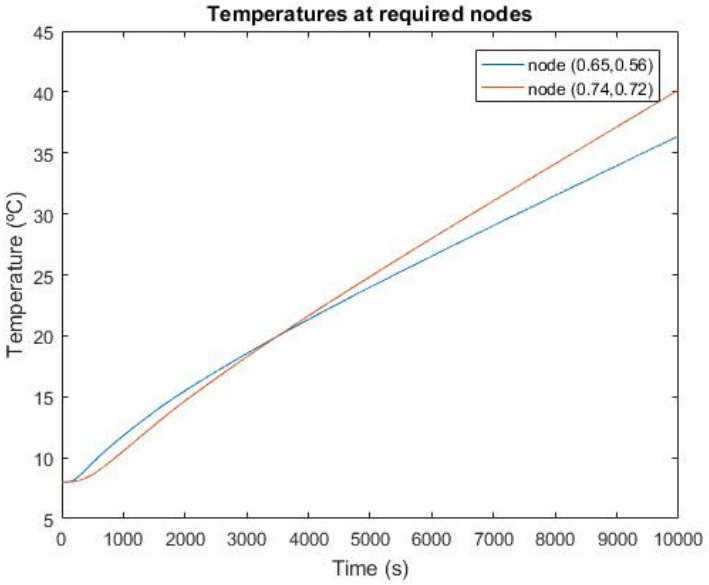

Figure 12: Temperatures at specified points

The red line shows the temperature at location (0.74,0.72), and the blue line shows the temperature at location (0.65,0.56). It makes sense, since these locations are near to the right wall where the temperature increases with time.

In figure 13 are compared the temperature maps between the known problem solution and the results obtained, at time t=5,000s. In this way, it is possible to check the results of the solution (figure 13(b)) with the results given in the statement (figure 13(a)).

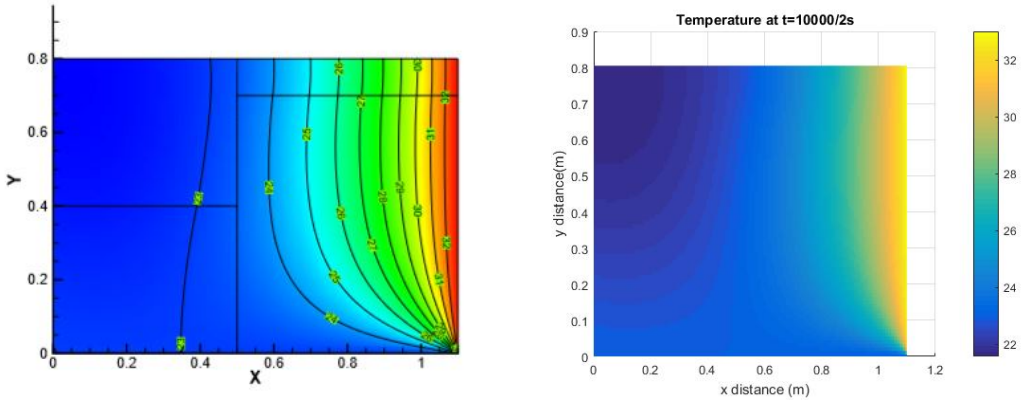

(a) Statement hint [5]

(b) Temperature at t=5,000s

Figure 13: Temperature check, Heat Transfer problem

2.4 Numerical resolution convection-diffusion equation

The general convection-diffusion equation is:

$$\frac{\partial(\rho\phi)}{\partial t} + \nabla \cdot (\rho\vec{v}\phi) = \nabla \cdot (\Gamma\nabla\phi) + S_\phi \tag{18}$$

Where 'ρ' refers to the density, '$\vec{v}$' to the velocity field and the other therms ('ϕ', 'Γ' and 'S_ϕ') can be referred to different variables as it is shown in table 5.

Equation	ϕ	Γ	S_ϕ
Mass conservation	1	0	0
Momentum	$\vec{v}$	μ	$-\nabla p + \nabla\vec{\tau} - \mu\nabla\vec{v} + \rho\vec{g}$
Energy (semiperfect gas)	u	λ/C	$-\nabla\dot{q}^n - p\nabla\vec{v} + \vec{\tau} : \nabla\vec{v}$

Table 5: Values of ϕ, ρ and S_ϕ for different equations

The aim of this section is to write a C++ code in order to solve the convection-diffusion equation numerically. To validate the script there will be 4 specific cases to study, which are the following ones [8]:

2.4.0.1 Unidimensional flow with an unidimensional variation of the variable solved in the same direction of the flow

The velocity field has only the component in 'x' direction, as it shown in equation 19.

$$\vec{v}(x,y) = \begin{pmatrix} U_o \\ 0 \end{pmatrix} \tag{19}$$

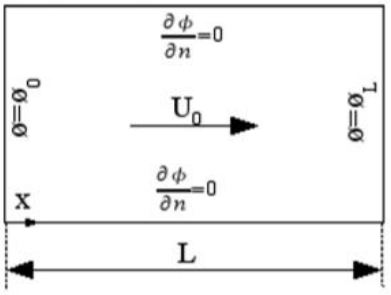

Figure 14: First case Convection-Diffusion [8]

Then, operating with equation 18 and considering a steady case, it is possible to figure out the analytical solution:

$$\frac{\phi - \phi_o}{\phi_L - \phi_o} = \frac{exp(Px/L) - 1}{exp(P) - 1} \tag{20}$$

Where P is the Peclet number:

$$P = \frac{\rho u L}{\Gamma} \tag{21}$$

2.4.0.2 Unidimensional flow with an unidimensional variation of the variable solved in the perpendicular direction of the flow

The second case has the same boundary conditions than the first one, but now changing the velocity field.

$$\vec{v}(x,y) = \begin{pmatrix} 0 \\ V_o \end{pmatrix} \tag{22}$$

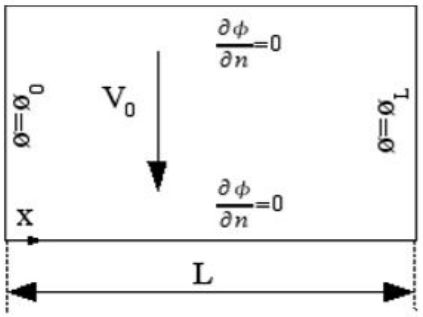

Figure 15: Second case Convection-Diffusion [8]

If the problem is considered steady, the analytical solution is:

$$\phi = \phi_o + \frac{\phi_L - \phi_o}{L} x \tag{23}$$

This solution is a straight line which join the values of the Dirichlet boundary conditions (where the values are known).

2.4.0.3 Diagonal flow

In this case, the velocity field is:

$$\vec{v}(x,y) = \begin{pmatrix} V_o \cdot \cos(\alpha) \\ V_o \cdot \sin(\alpha) \end{pmatrix} \tag{24}$$

Now the boundary conditions are that all the values at the walls are known (Dirichlet).

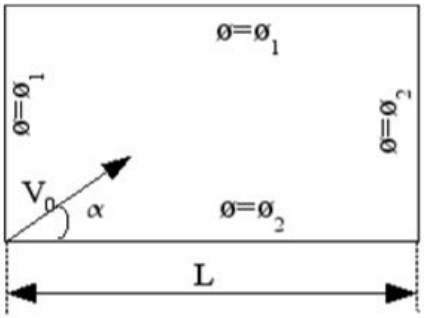

Figure 16: Third case Convection-Diffusion [8]

If the Peclet number tends to infinite, the solution above the diagonal is ϕ_1 and ϕ_2 below the diagonal.

2.4.0.4 Solenoidal flow

Fourth case is also known as the 'Smith-Hutton problem', and it is described in figure 17. The velocity field is:

$$\vec{v}(x,y) = \begin{pmatrix} 2y(1-x^2) \\ -2x(1-y^2) \end{pmatrix} \tag{25}$$

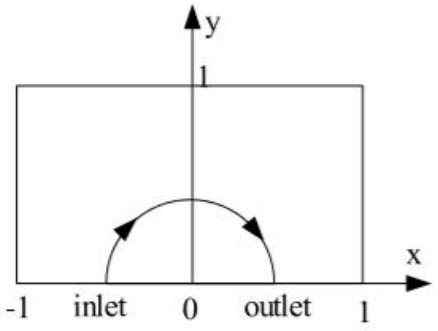

Figure 17: Fourth case Convection-Diffusion [8]

In this case, the boundary conditions are shown in table 6

$-1 < x < 0$	y=0	$\phi = 1 + \tanh[(2x+1)\alpha]$
x=-1	$0 < y < 1$	$\phi = 1 - \tanh[\alpha]$
$0 < x < 1$	y=0	$\frac{\partial \phi}{\partial y} = 0$
$-1 < x < 1$	y=1	$\phi = 0$
x=1	$0 < y < 1$	$\phi = 0$

Table 6: Boundary conditions Smith-Hutton

2.4.1 Equations and schemes

Considering the control volume of the picture 4, equation 18 can be written as equation 26.

$$\begin{aligned} &\frac{\rho_P \phi_P - \rho_P^o \phi_P^o}{\Delta t} V_P + \dot{m}_e \phi_e - \dot{m}_w \phi_w + \dot{m}_n \phi_n - \dot{m}_s \phi_s \\ &= D_e(\phi_E - \phi_P) - D_w(\phi_P - \phi_W) + D_n(\phi_N - \phi_P) - D_s(\phi_P - \phi_S) + S_{\phi P} V_P \end{aligned} \tag{26}$$

$$D_x = \Gamma_x \frac{S_x}{d_{PX}} \qquad where \rightarrow \begin{pmatrix} x = n, s, e, w \\ X = N, S, E, W \end{pmatrix} \tag{27}$$

The mass conservation equation in this domain is:

$$\frac{\rho_P - \rho_P^o}{\Delta t} V_P + \dot{m}_e - \dot{m}_w + \dot{m}_n - \dot{m}_s = 0 \tag{28}$$

If equation 28 is multiplied by ϕ_P and then is subtracted from equation 26, it yields to equation 29. This equation works with the density of the previous instant and becomes easier [9].

$$\begin{aligned} &\rho_P^o \frac{\phi_P - \phi_P^o}{\Delta t} V_P + \dot{m}_e(\phi_e - \phi_P) - \dot{m}_w(\phi_w - \phi_P) + \dot{m}_n(\phi_n - \phi_P) - \dot{m}_s(\phi_s - \phi_P) \\ &= D_e(\phi_E - \phi_P) - D_w(\phi_P - \phi_W) + D_n(\phi_N - \phi_P) - D_s(\phi_P - \phi_S) + S_{\phi P} V_P \end{aligned} \tag{29}$$

However, as the cases to study are steady, it is not necessary to use this kind of discretization.

It is important to remind that the terms with subscripts 'e,w,n,s' refers to the values at the cell faces of the control volume (see figure 4). It means that the mass flow is the one evaluated at the cell face (considering that velocity field and density are known), but the values of $\phi_{e,w,n,s}$ must be carefully taken into account. There are some schemes to do it, and the simplest ones are [9]:

- Central Difference Skin (CDS): This is a second order scheme, which can provide some problems in the convergence of the solution. It consists in a linear interpolation between the values of the nodes:

$$\phi_e - \phi_P = f_e(\phi_E - \phi_P) \qquad where \;\; f_e = \frac{d_{Pe}}{d_{PE}} \tag{30}$$

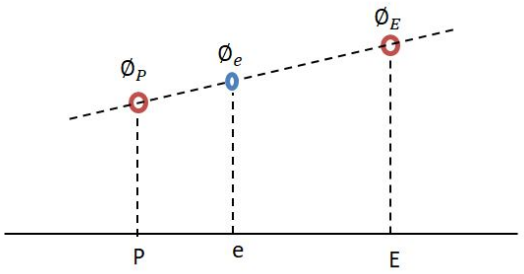

Figure 18: Central Difference Skin

- Upwind Difference Skin (UDS): This scheme adjudge the value of the node where the mass flow is coming from.

$$\phi_e - \phi_P = f_e(\phi_E - \phi_P) \qquad where \quad \begin{matrix} f_e = 0 & if & \dot{m}_e > 0 \\ f_e = 1 & if & \dot{m}_e < 0 \end{matrix} \tag{31}$$

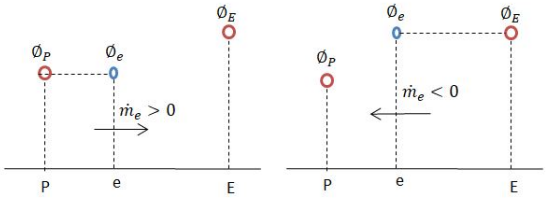

Figure 19: Upwind Difference Skin

- Exponential Difference Skin (EDS): This is a second/third order scheme. The value of ϕ is calculated with equation 18 simplified (considering steady, 2D and $S_\phi = 0$). Then it is possible to find the analytical solution, which is used to evaluate $\phi_{e,w,n,s}$.

$$\phi_e - \phi_P = \frac{exp(P_e \frac{d_{Pe}}{d_{PE}}) - 1}{exp(P_e) - 1}(\phi_E - \phi_P) \qquad where \;\; P_e = \frac{\rho_e v_{xe} d_{PE}}{\Gamma_e} \tag{32}$$

However, higher order schemes are presented, since they are necessary to solve high Reynolds numbers in this thesis. The following information is extracted from [10] and [11].

- QUICK: QUICK stands for Quadratic Upstream Interpolation for Convective Kinematics. As it has been said, it is a high order scheme used to solve the convection-diffusion. This scheme uses three nodes to do the interpolation in order to get the value at the cell face (see figure 20).

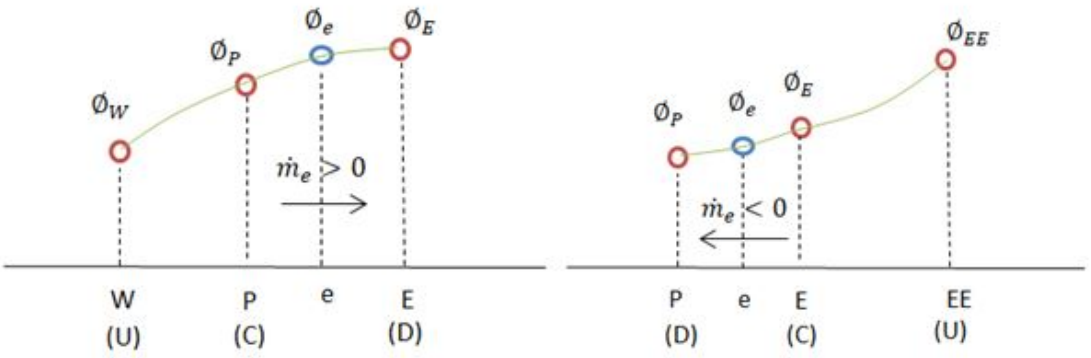

Figure 20: QUICK scheme illustration

Once the mass flow has been calculated, and the nodes which will be used are already known, it is easier to work with the dimensionless variables shown in equation 33.

$$\hat{\phi} = \frac{\phi - \phi_U}{\phi_D - \phi_U} \qquad \hat{x} = \frac{x - x_U}{x_D - x_U} \tag{33}$$

Then, the dimensionless velocity at the cell face is computed with equation 34.

$$\hat{\phi}_e = \hat{x}_e + \frac{\hat{x}_e(\hat{x}_e - 1)}{\hat{x}_C(\hat{x}_C - 1)}(\hat{\phi}_C - \hat{x}_C) \tag{34}$$

- SMART:Using the dimensionless variables shown in equation 33, SMART scheme is computed as equations 35.

$$\begin{aligned}
&\hat{\phi}_e = -\frac{\hat{x}_e(1 - 3\hat{x}_C + 2\hat{x}_e)}{\hat{x}_C(\hat{x}_C - 1)}\hat{\phi}_C && 0 < \hat{\phi}_C < \frac{\hat{x}_C}{3} \\
&\hat{\phi}_e = -\frac{\hat{x}_e(2\hat{x}_e - \hat{x}_C)}{1 - \hat{x}_C} + \frac{\hat{x}_e(2\hat{x}_e - 1)}{\hat{x}_C(\hat{x}_C - 1)}\hat{\phi}_C && \frac{\hat{x}_C}{3} < \hat{\phi}_C < \frac{\hat{x}_C}{\hat{x}_e}(1 + \hat{x}_e - \hat{x}_C) \\
&\hat{\phi}_e = 1 && \frac{\hat{x}_C}{\hat{x}_e}(1 + \hat{x}_e - \hat{x}_C) < \hat{\phi}_C < 1 \\
&\hat{\phi}_e = \hat{U}_C && elsewhere
\end{aligned} \tag{35}$$

The code developed in this section uses the Upwind Difference Skin, although other schemes will be used in this thesis. The equation which has to be solved is the following (equation 36):

$$a_P\phi_P = a_E\phi_E + a_W\phi_W + a_N\phi_N + a_S\phi_S + b_P \tag{36}$$

Where, considering the axis directions and a steady problem, the coefficients are:

$$a_E = D_e - \dot{m}_e f_e \qquad where \begin{cases} f_e = 0 & \text{if } \dot{m}_e > 0 \\ f_e = 1 & \text{if } \dot{m}_e < 0 \end{cases} \tag{37a}$$

$$a_W = D_w + \dot{m}_w f_w \qquad where \begin{cases} f_w = 0 & \text{if } \dot{m}_w < 0 \\ f_w = 1 & \text{if } \dot{m}_w > 0 \end{cases} \tag{37b}$$

$$a_N = D_n - \dot{m}_n f_n \qquad where \begin{cases} f_n = 0 & \text{if } \dot{m}_n > 0 \\ f_n = 1 & \text{if } \dot{m}_n < 0 \end{cases} \tag{37c}$$

$$a_S = D_s + \dot{m}_s f_s \qquad where \begin{cases} f_s = 0 & \text{if } \dot{m}_s < 0 \\ f_s = 1 & \text{if } \dot{m}_s > 0 \end{cases} \tag{37d}$$

$$a_P = a_E + a_W + a_N + a_S + \dot{m}_e + \dot{m}_n - \dot{m}_w - \dot{m}_s \tag{37e}$$

Notice that the criteria in equations 37a and 37c is the opposite of equations 37b and 37d. This is because of the sign directions used in the control volume. A negative value of $\dot{m}_w$ means that the mass flow is exiting from the control volume (the same happens with $\dot{m}_s$), while negative values of $\dot{m}_e$ and $\dot{m}_n$ mean that the mass flow is entering.

2.4.2 Boundary conditions

There are two kind of boundary conditions[9]:

- Dirichlet: The value at the boundary is known ($\phi_w = \phi_W$).

$$\left.\frac{\partial \phi}{\partial x}\right|_w \approx \frac{\phi_P - \phi_w}{d_{Pw}} \tag{38}$$

- Neumann: The derivative at the boundary is known ($\Gamma_w \left.\frac{\partial \phi}{\partial x}\right|_w = j_w$).

$$j_w \approx \Gamma_w \frac{\phi_P - \phi_w}{d_{Pw}} \qquad \rightarrow \qquad \phi_w = \phi_P - \frac{j_w d_{Pw}}{\Gamma_w} \tag{39}$$

Equations 38 and 39 are necessary to work with the boundary nodes.

2.4.3 Script convection-diffusion equation

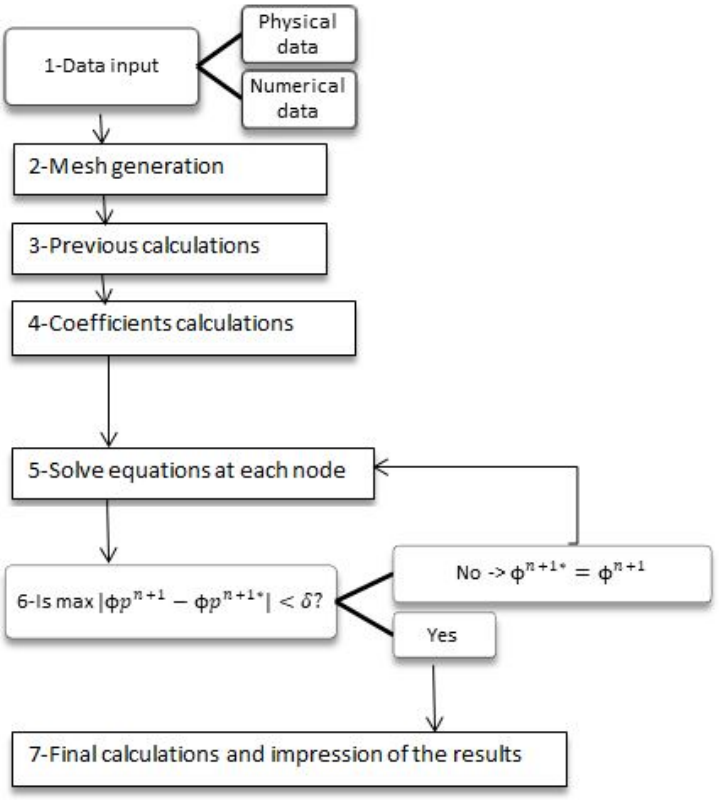

Figure 21: Script convection-diffusion

1. All data input
   - Physical data: geometry, density (ρ), gamma (Γ) ...
   - Numerical data: convergence factor (δ), number of divisions, relaxation factor...
2. Mesh generation: Generates the mesh of nodes.
3. Previous calculations: Mainly computes the velocities map, and sets the boundary conditions of the problem.
4. Coefficients calculations: Save the value of the coefficients shown in equations 37 for each node .
5. Solve the equations shown in section 2.4.1 in order to figure out the value of ϕ at each node.
6. Check the convergence of the solution founded.
   - If solution has not converged $\rightarrow$ go to step 5 with the new ϕ map.
   - If solution has converged $\rightarrow$ next step.
7. Final calculations and impression of the results.

2.4.4 Results convection-diffusion problems

2.4.4.1 Mesh study

Since the problems are steady, there is no time discretization. It means that the only study of the mesh is related to the geometry discretization. This study is done considering the problem of section 2.4.0.1, because the analytical solution is known and it is not linear.

The configuration of the problem yields to a variation of ϕ only in the 'x' axis direction (see equation 20). The discretization is studied in this axis, and then the same criteria is applied in the 'y' direction.

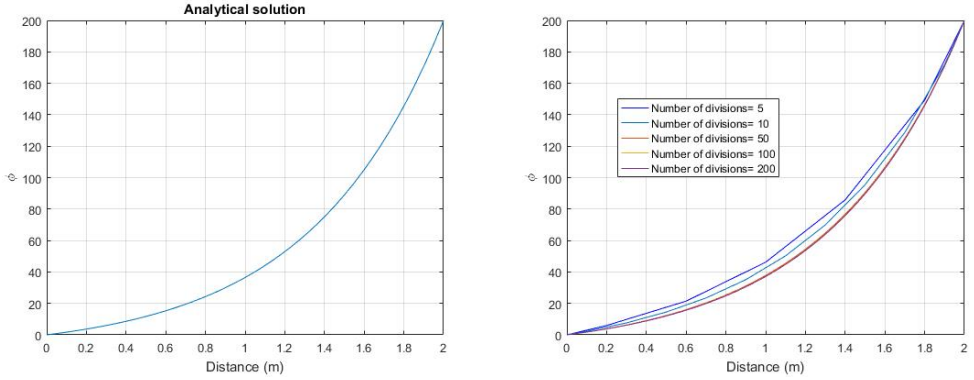

(a) Analytical solution (b) Numerical solution

Figure 22: Comparison between analytical and numerical solution - first case convection-diffusion

Figure 22 shows both solutions: analytically (22(a)) and numerically (figure 22(b)). It is possible to see that from divisions highers than 50, the solution has converged. Then, figure 23 shows the error (see equation 40) in front of the number of divisions. However, the final number of divisions got for the results is 200, since the problem is steady and the computational cost is low enough to use this discretization.

$$error = \sqrt{\frac{1}{\text{number of divisions}} \sum (\phi_{numeric} - \phi_{analytic})^2} \tag{40}$$

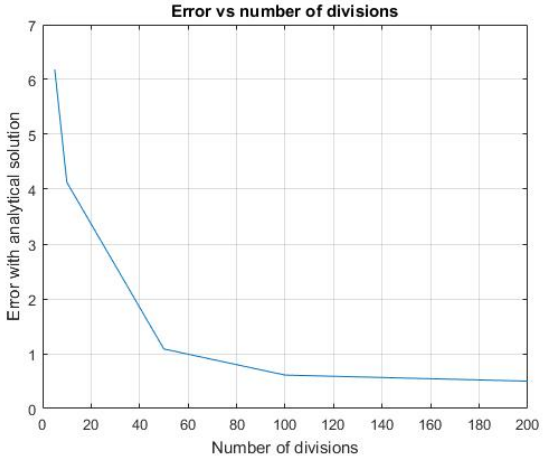

Figure 23: Error vs number of divisions

2.4.4.2 Results problem 'Unidimensional flow with a unidimensional variation of the variable solved in the same direction of the flow'

As it has been said, this problem has an analytical solution (equation 20) which depends on the boundary conditions and the Peclet number.

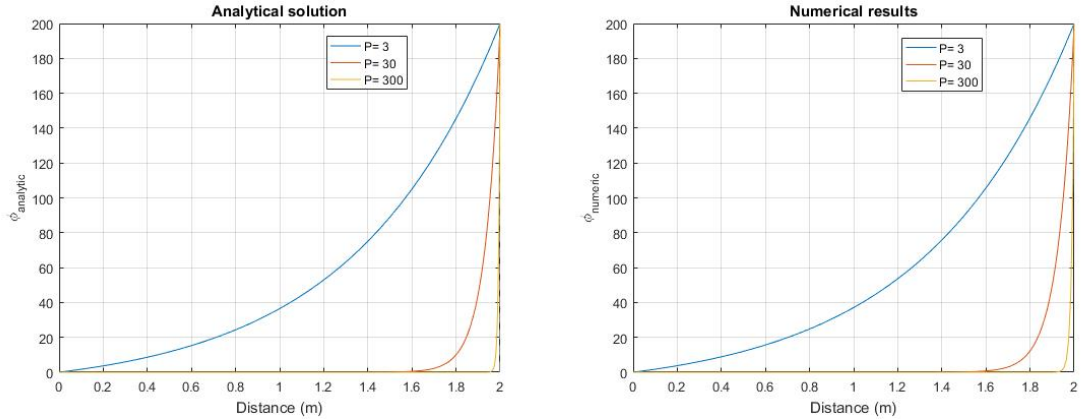

(a) Analytic solution for different Peclet numbers

(b) Numerical solution for different Peclet numbers

Figure 24: Solutions first case convection-diffusion

Figure 24 shows the analytical and numerical solution with differents Peclet numbers. However, increasing Peclet number increases also the error between both solutions (see figure 25).

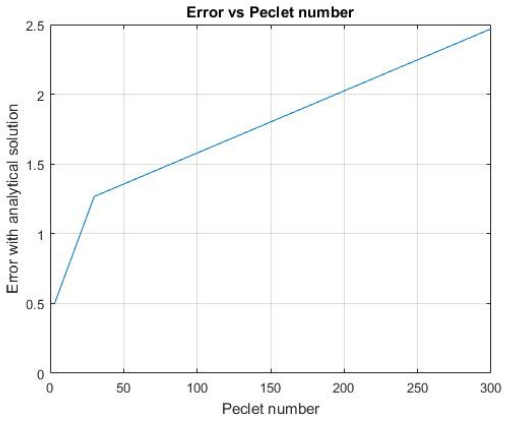

Figure 25: Error vs Peclet number in first case

2.4.4.3 Results problem 'Unidimensional flow with a unidimensional variation of the variable solved in the perpendicular direction of the flow'

This second case has also an analytical solution (see equation 23), which is a straight line joining the boundary conditions from 'x=0' to 'x=L'. It means that the discretization used here does not matter, since it will be always given the same straight line.

It is also important to notice that equation 23 only depends on the boundary conditions, and the velocity field is irrelevant.

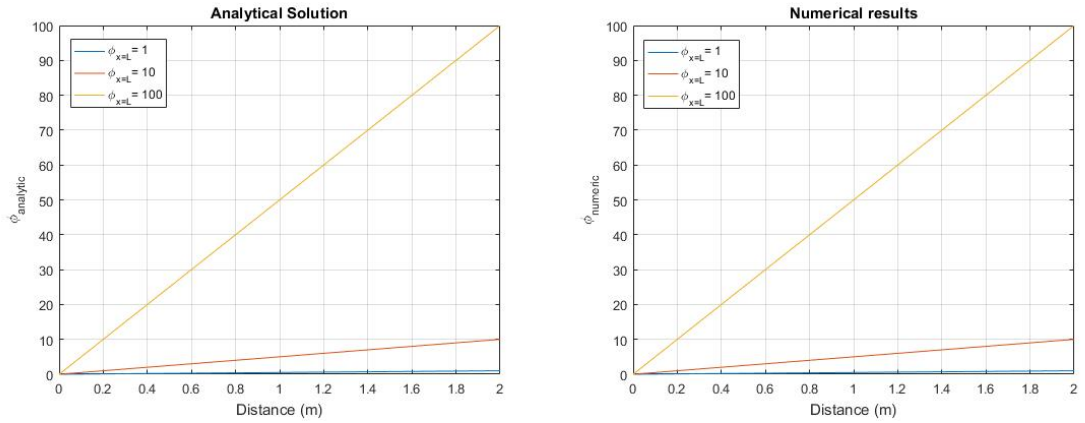

(a) Analytic solution for different boundary conditions (b) Numerical solution for different boundary conditions

Figure 26: Solutions second case convection-diffusion

2.4.4.4 Results problem 'Diagonal flow'

In this case it is known that if the Peclet number tends to infinite, the solution above the diagonal is equal to ϕ_1 and above the diagonal to ϕ_2 (see figure 16).

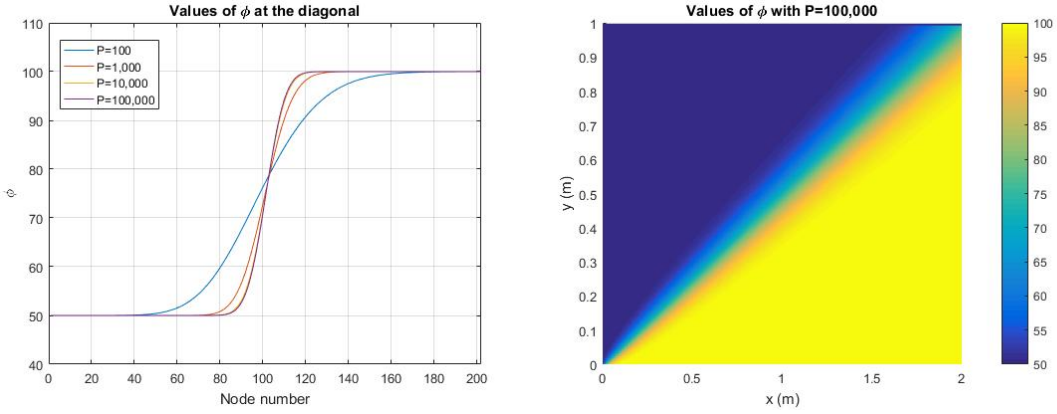

(a) Values of ϕ at the diagonal with different Peclet numbers

(b) Values of ϕ with Peclet=100,000

Figure 27: Solutions third case convection-diffusion - diagonal flow

Figure 27(a) shows the evolution of ϕ along the diagonal. Higher the Peclet number studied, higher the slope of the ϕ variation.

2.4.4.5 Results problem 'Solenoidal flow'

The problem of section 2.4.0.4 is also known as the Smith-Hutton problem. The solutions at the outlet are known for different relations of ρ/Γ (see table 7) .

x	$\rho/\Gamma = 10$	$\rho/\Gamma = 1,000$	$\rho/\Gamma = 1,000,000$
0.0000	1.9890	2.0000	2.0000
0.1000	1.4020	1.9900	2.0000
0.2000	1.1460	1.9997	2.0000
0.3000	0.9460	1.9850	1.9990
0.4000	0.7750	1.8410	1.9640
0.5000	0.6210	0.9510	1.0000
0.6000	0.4800	0.1540	0.0360
0.7000	0.3490	0.0010	0.0010
0.8000	0.2270	0.0000	0.0000
0.9000	0.1110	0.0000	0.0000
1.0000	0.0000	0.0000	0.0000

Table 7: Solution Smith-Hutton [8]

Then, figure 28 shows the results given by the script developed compared with the solution table 7.

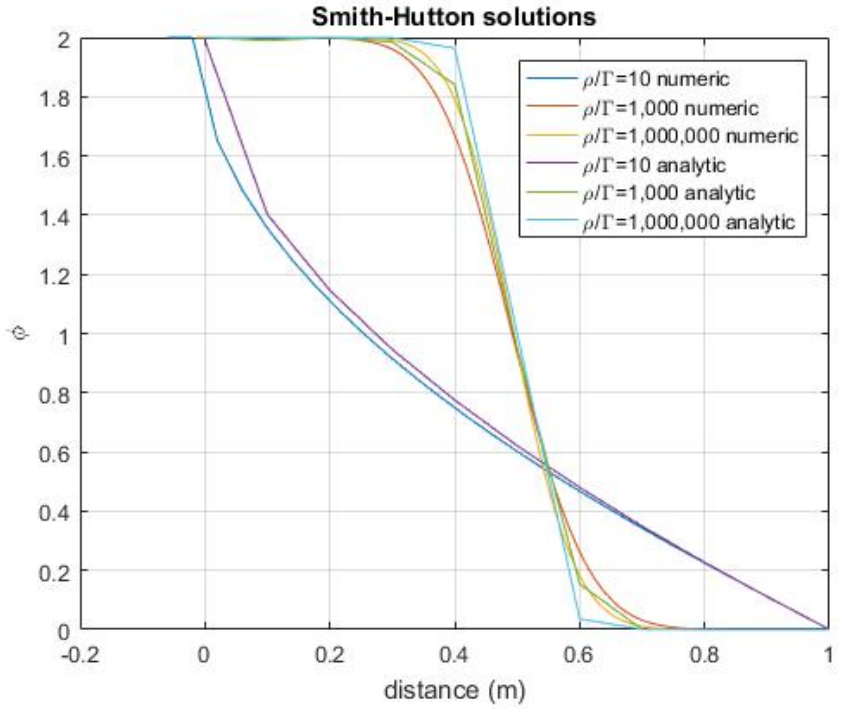

Figure 28: Solution check Smith-Hutton problem

Figures 29(a),29(b) and 29(c) represents the values of ϕ plotted in surfaces, for different values of ρ/Γ and different views.

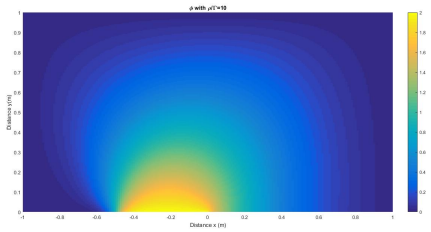

(a) ϕ with $\rho/\Gamma = 10$

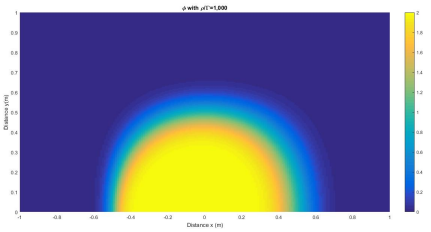

(b) ϕ with $\rho/\Gamma = 1,000$

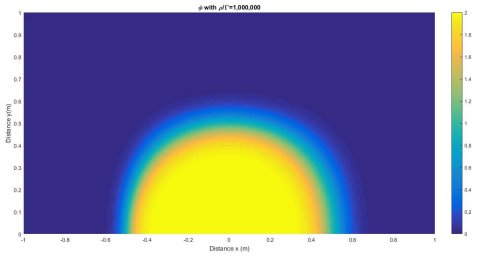

(c) ϕ with $\rho/\Gamma = 1,000,000$

Figure 29: Solutions Smith-Hutton plotted

2.5 Conclusions

These firsts steps inside the numerical methods have been useful to realize the complexity that implies. The pure diffusion difficulty in the heat transfer problem is mainly related to the geometry discretization needed and the fact that is unsteady. On the other hand, despite the convection-diffusion problems treated are steady, the complexity remains in the convective term, which must be calculated through the schemes shown.

It is important to mention that the importance of these problems is related to the validation of the codes which will be used to solve Navier-Stokes. The results obtained until now are not such important, since they are only useful to check the codes written.

3 Fractional Step Method

3.1 Introduction

This section explains the bases of the 'Fractional Step Method', from now called 'FSM'. First of all, there is a theory explanation of this method and the theorem which allows its application: The Helmholtz-Hodge theorem.

Then is shown a physical problem which has to be taken into account before use FSM. This problem is solved through a special discretization based on the utilization of staggered meshes. Once it has been explained, the basic script structure is shown.

3.2 Fractional Step Method (FSM) theory explanation

FSM is an explicit method commonly used to solve the incompressible Navier-Stokes equations [12]. Its success is because of the code simplicity and the performance compared with other methodologies.

First of all, it is necessary to talk about the Helmholtz-Hodge theorem.

Theorem: *A given field ω, defined in a bounded domain Ω with smooth boundary $\delta\Omega$, is uniquely decomposed in a pure gradient field and a divergence-free vector parallel to $\delta\Omega$*

$$\omega = a + \nabla\phi \qquad where \qquad \nabla \cdot a = 0 \quad a \in \Omega \tag{41}$$

The theorem also applies for periodic inflow/outflow conditions.

As it has been said, the equations used to develop the script are the mass and linear momentum conservation. Then, it is also considered that the flow is incompressible. The resultant equations are:

$$\nabla \cdot \vec{v} = 0 \tag{42}$$

$$\rho\frac{\partial \vec{v}}{\partial t} + (\rho\vec{v}\cdot\nabla)\vec{v} = -\nabla p + \mu\Delta\vec{v} \tag{43}$$

Then, 'R' is defined as:

$$\vec{R}(\vec{v}) = -(\rho\vec{v}\cdot\nabla)\vec{v} + \mu\Delta\vec{v} \tag{44}$$

Integrating the momentum equation:

$$\int_{t^n}^{t^{n+1}} \rho\frac{\partial \vec{v}}{\partial t}dt = \int_{t^n}^{t^{n+1}} \vec{R}(\vec{v})dt - \int_{t^n}^{t^{n+1}} \nabla p dt \tag{45}$$

$$\rho(\vec{v}^{n+1} - \vec{v}^n) = \vec{R}(\vec{v})^{n+\frac{1}{2}}\Delta t - \nabla p^{n+\frac{1}{2}}\Delta t \tag{46}$$

Interpolating:

$$\frac{\vec{R}(\vec{v}^{n+\frac{1}{2}}) - \vec{R}(\vec{v}^n)}{(n+\frac{1}{2}) - n} = \frac{\vec{R}(\vec{v}^n) - \vec{R}(\vec{v}^{n-1})}{n-(n-1)} \tag{47}$$

$$\vec{R}(\vec{v}^{n+\frac{1}{2}}) = \frac{3}{2}\vec{R}(\vec{v}^n) - \frac{1}{2}\vec{R}(\vec{v}^{n-1}) \tag{48}$$

The Navier Stokes equations integrated are:

$$\nabla \cdot \vec{v}^{n+1} = 0 \tag{49}$$

$$\rho\frac{\vec{v}^{n+1} - \vec{v}^n}{\Delta t} = \frac{3}{2}\vec{R}(\vec{v}^n) - \frac{1}{2}\vec{R}(\vec{v}^{n-1}) - \nabla p^{n+1} \tag{50}$$

Through the Helmholtz-Hodge it is possible to get the unique decomposition shown in equation 51.

$$\vec{v}^p = \vec{v}^{n+1} + \frac{\Delta t}{\rho}\nabla p^{n+1} \tag{51}$$

Notice that equation 51 satisfy the Helmholtz-Hodge theorem since the flow is incompressible ($\nabla \cdot \vec{v^{n+1}} = 0$). Replacing the values of equation 50 by the ones of equation 51, it yields to equation 52.

$$\rho\frac{\vec{v}^p - \vec{v}^n}{\Delta t} = \frac{3}{2}\vec{R}(\vec{v}^n) - \frac{1}{2}\vec{R}(\vec{v}^{n-1}) \tag{52}$$

In equation 52 the only unknown value is $\vec{v}^p$, so it is possible to isolate and solve explicitly. Once it is done, the next step is to calculate the pressure field. In order to do that, equation 51 is derived. Considering that the flow is incompressible, Poisson equation 53 is achieved.

$$\Delta p^{n+1} = \frac{\rho}{\Delta t}\nabla \cdot \vec{v}^p \tag{53}$$

Then, once the Poisson equation is solved, it is possible to calculate the velocity field at the instant n+1 through equation 51.

1. Evaluation of $\vec{R}(\vec{v}^n)$
2. $\vec{v}^p = \vec{v}^n + \frac{\Delta t}{\rho}[\frac{3}{2}\vec{R}(\vec{v}^n) - \frac{1}{2}\vec{R}(\vec{v}^{n-1})]$
3. $\Delta p^{n+1} = \frac{\rho}{\Delta t}\nabla \cdot \vec{v}^p$
4. $\vec{v}^{n+1} = \vec{v}^p - \frac{\Delta t}{\rho}\nabla p^{n+1}$

3.3 The checkerboard problem

When the velocity field is computed through the predictor velocities, it is necessary to calculate the pressure gradient at each node. Supposing only the 'x' direction, and isolating the velocity at instant t=n+1 from equation 51, it yields to equation 54.

$$u_P^{n+1} = u_P^p - \frac{\Delta t}{\rho}(\frac{p_E^{n+1} - p_W^{n+1}}{2\Delta x}) \tag{54}$$

The problem in equation 54 is that the gradient of pressure at node P is independent of the pressure at node P. It can generate a nonphysical pressure distribution despite the velocity field has converged.

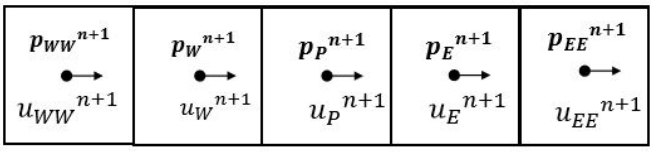

Figure 30: Checkerboard problem example [13]

$$p_{WW} = 100 \quad p_W = 0 \quad p_P = 100 \quad p_E = 0 \quad p_{EE} = 100$$

Considering the values below figure 30, it can be observed that verifies $\nabla p^{n+1} = 0$ although it is nonphysical solution.

A possible solution to this problem is to use staggered meshes. In this way, it is possible to avoid the checkerboard problem, but it becomes very complex when the mesh is unstructured.

3.4 Staggered meshes

Figure 31 is a basic example of the staggered meshes.

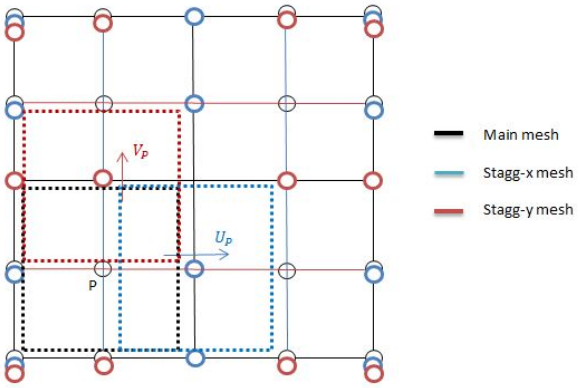

Figure 31: Staggered meshes illustration

The main mesh is only used to get the pressure field. Then, it is easy to see that the nodes which belong to the main mesh are located at the cell faces of the staggered meshes. It enables to compute the pressure gradient at the determined node of the staggered mesh, since it is exactly in the middle between the two main mesh's nodes. Doing this, checkerboard problem is avoid. However, it means that all the 'x' components of the velocity will be achieved in the staggered 'x' mesh, and the 'y' components in the staggered 'y' mesh.

3.5 Code equations

As it has been said, the first step of the solver is to obtain the values of R in both directions. Since now, 'u' is referred to the 'x' component of the velocity and 'v' to the vertical direction. It is also important to realize that both components are computed considering different meshes (see figure 31).

$$\begin{aligned} R(u)V_{CV} = &-(\dot{m}_e u_e - \dot{m}_w u_w + \dot{m}_n u_n - \dot{m}_s u_s) + \left(\mu_e \frac{u_E - u_P}{d_{EP}} S_e \right. \\ &\left. + \mu_n \frac{u_N - u_P}{d_{NP}} S_n + \mu_w \frac{u_W - u_P}{d_{WP}} S_w + \mu_s \frac{u_S - u_P}{d_{SP}} S_s \right) \end{aligned} \tag{55a}$$

$$\begin{aligned} R(v)V_{CV} = &-(\dot{m}_e v_e - \dot{m}_w v_w + \dot{m}_n v_n - \dot{m}_s v_s) + \mu \left(\mu_e \frac{v_E - v_P}{d_{EP}} S_e \right. \\ &\left. + \mu_n \frac{v_N - v_P}{d_{NP}} S_n + \mu_w \frac{v_W - v_P}{d_{WP}} S_w + \mu_s \frac{v_S - v_P}{d_{SP}} S_s \right) \end{aligned} \tag{55b}$$

Equations 55 have some subscripts with capital letters and others with small letters. As it has been done until now, capital letters refers to the values at the nodes and small letters refers to the values at the cell face. It means that the mass flows and the velocities at the cell faces must be calculated through a convection-diffusion scheme.

The code developed uses a high order scheme in order to obtain accurate results. It is known that increasing the Reynolds number convection domains above diffusion, and false diffusion can

affect the results. QUICK is the main scheme used, but it is compared with SMART and UDS (which is used in convection-diffusion problems).

Now it is possible to calculate the value of R for both staggered meshes. The next step is to obtain the predictor velocities isolating them from equation 52, and it yields to equations 56.

$$u^p = u^n + \frac{\Delta t}{\rho}\left[\frac{3}{2}R(u^n) - \frac{1}{2}R(u^{n-1})\right] \tag{56a}$$

$$v^p = v^n + \frac{\Delta t}{\rho}\left[\frac{3}{2}R(v^n) - \frac{1}{2}R(v^{n-1})\right] \tag{56b}$$

When both predictor velocities fields are got, it enables to calculate the pressure field through Poisson equation 53, that can be discretized as equation 57.

$$a_P p_P^{n+1} = a_E p_E^{n+1} + a_N p_N^{n+1} + a_S p_S^{n+1} + a_W p_W^{n+1} + b_P \tag{57}$$

$$a_E = \frac{A_e}{d_{EP}} \qquad a_N = \frac{A_n}{d_{NP}}$$

$$a_W = \frac{A_w}{d_{WP}} \qquad a_S = \frac{A_s}{d_{SP}}$$

$$b_P = -\frac{\rho}{\Delta t}[u_e^p A_e - u_w^p A_w + u_n^p A_n - u_s^p A_s]$$

The geometry of the coefficients shown belongs to the main mesh, since is the one used to compute the pressure field.

In order to solve equation 57 it is necessary to use any linear solver. The code developed uses a Gauss-Seidel linear solver, which calls a relaxation factor in case of the convergence is not got. It is also set a pressure value in a single node to help the stability of the solver. Notice that the real pressure value is not important, but the gradient.

Once the pressure field is achieved, it is possible to calculate the velocities at the staggered meshes through equation 51. Checkerboard problem is avoid because the pressure field gives the values at the cell faces of the staggered meshes.

$$u_P^{n+1} = u_P^p - \frac{\Delta t}{\rho} \cdot \frac{p_B^{n+1} - p_A^{n+1}}{d_{BA}} \tag{58a}$$

$$v_P^{n+1} = v_P^p - \frac{\Delta t}{\rho} \cdot \frac{p_B^{n+1} - p_A^{n+1}}{d_{BA}} \tag{58b}$$

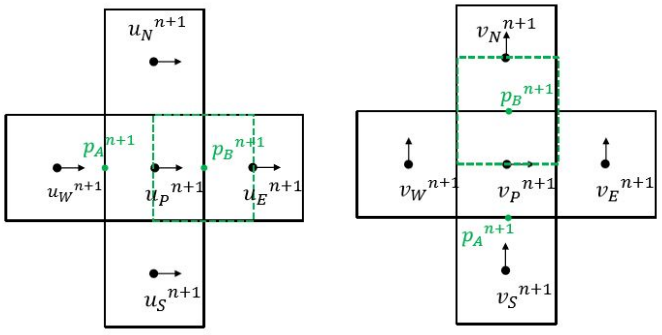

(a) stagg-x mesh (b) stagg-y mesh

Figure 32: Computing velocities from pressure field in staggered meshes [13]

The last task is to choose the next time step. It is important to follow some criteria here, because the convergence to a steady solution will depend on it. Literature gives the following rule (Courant-Friedrich-Levy)[12]:

$$\begin{aligned} t_{step-c} &= min\left(0.35\frac{\Delta x}{|v|}\right) \\ t_{step-d} &= min\left(0.20\frac{\rho\Delta x^2}{\mu}\right) \\ t_{step} &= min(t_{step-c}, t_{step-d}) \end{aligned} \tag{59}$$

3.6 Description of the code

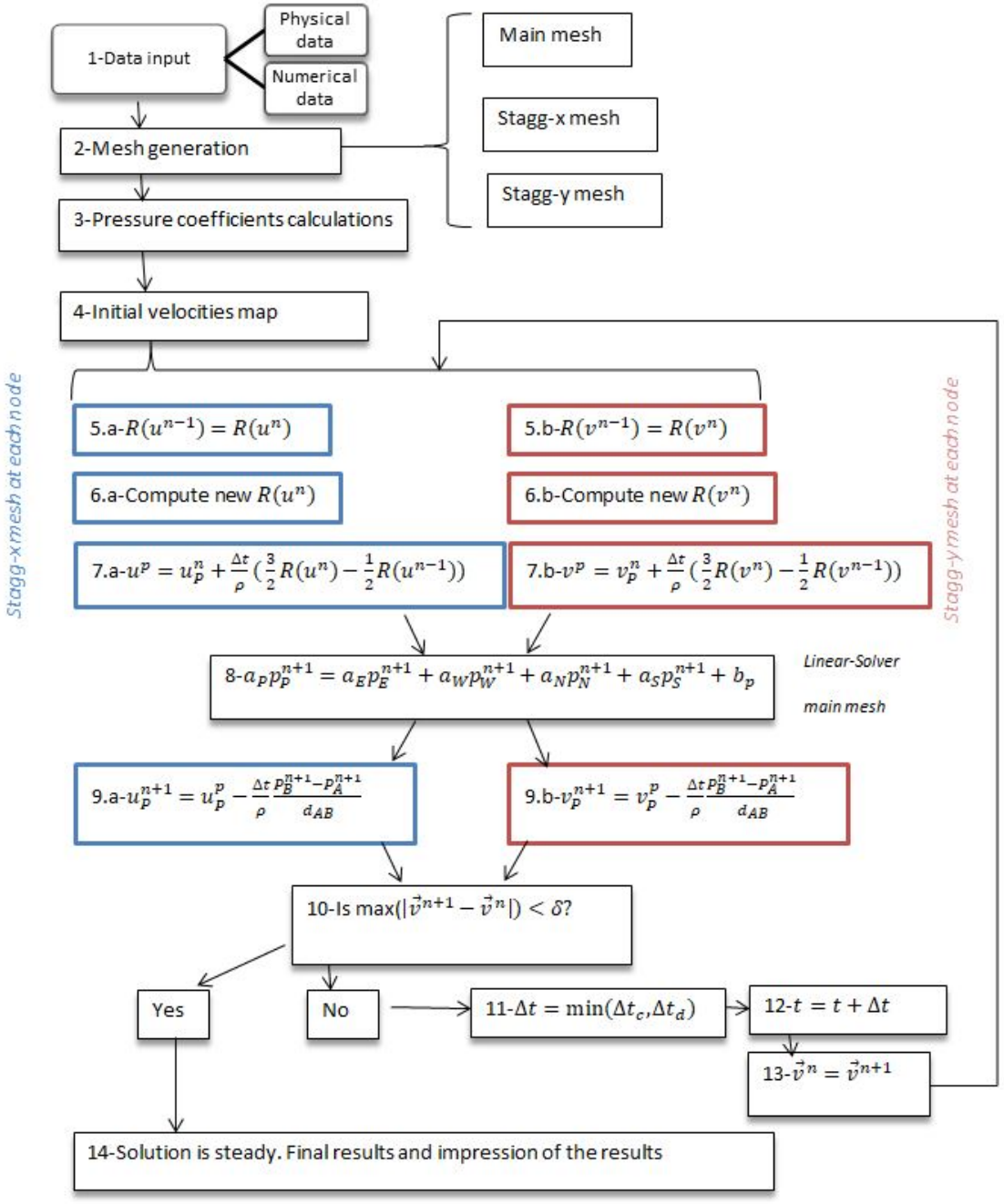

Figure 33: Fractional Step Method code scheme

1. Input data:
   - Physical data: Reynolds number. Then, the other variables are calculated with relation 60.
   $$Re = \frac{\rho \cdot L \cdot u_{ref}}{\mu} \tag{60}$$
   - Numerical data: Number of divisions, relaxation factor, convergence criteria (δ)...

2. Mesh generation: Since the code is working with staggered meshes, it is necessary to compute 3 meshes (see figure 33). Each mesh has to have the following data: positions of the nodes, areas of the cell faces and volumes.

3. Pressure coefficients calculations: Most of the coefficients of equation 57 are constant, and they can be calculated through the main mesh's geometry. The only coefficient that will change at each time step is b_P, which has to be computed every time iteration.

4. Initial velocities map: The values of the initial velocities for each staggered mesh have to be set.

5. For each staggered mesh at each node, safe the value of R in the previous instant.

6. Compute the new value of R at current instant. Here it is used the QUICK scheme mentioned before, in order to get the velocities at the cell faces. If it is done with a lower order scheme the results could be incorrect.

7. Calculate the predictor velocities for each staggered mesh. These three lasts steps can be done node by node, so it is only necessary to do one iteration.

8. Compute the pressure field. With the predictor velocities is possible to calculate the coefficients b_P at each time step, and the resultant linear equations are solved through a linear solver.

9. New velocity field. With the predictor velocities and the pressure field at time 'n+1' it is possible to get the new velocity field for each staggered mesh.

10. Compare the new velocity field with the previous one. If the solution becomes steady, then the velocity field will not change enough and the solver will stop. Otherwise, if the new velocity field changes more than the criteria established (δ), the solver will continue with a new time step.

11. If the solution is still unsteady, new time step has to be chosen following the criteria of Courant-Friedrich-Levy. In case of working with high Reynolds number, the time step is reduced in order to achieve the convergence to a steady solution.

12. Go to next time calculations.

13. Set the actual velocity field to start from step 5.

14. If the solution is steady, get the final results.

3.7 Conclusions

Despite the fact of the necessity of introducing the staggered meshes, the FSM seems to be an easy way to work with the Navier-Stokes equations. However, it has the disadvantage of an explicit method: the time step required to prevent the divergence is low.

4 Code verification and analysis of the numerical solutions. Internal and external flows

4.1 Introduction

This section presents different problems related to internal and external flows. Their solutions are shown and analysed, comparing with literature and analytical results to ensure their validity.

The first problem is called 'Lid-Driven Cavity'. As its name indicates, it consists in a cavity whose top wall is moving with a constant velocity. Its solution is known for different Reynolds numbers, and it is useful to check the script developed with the FSM.

Then it is studied the flow between flat plates, whose analytical solution is known. Checking this kind of flow allows to simulate solid bodies between the flat plates. A method called 'blocking-off' is used to create the solid part of the domain, starting with a square cylinder. There is literature related to this kind of solid, so it can be compared with known results. Moreover, with blocking-off method is possible to create other complex geometries without increasing the complexity of the code. In order to show that, the basic results for a rhombus, circular cylinder and a symmetric NACA profile are shown.

4.2 'Lid-Driven Cavity'

4.2.1 Description of the problem

The 'Lid-Driven Cavity' problem is commonly used to check the validity of a code developed to solve Navier-Stokes equations. It consists in a two dimensional cavity whose top wall is moving with constant velocity, and the other walls are fixed.

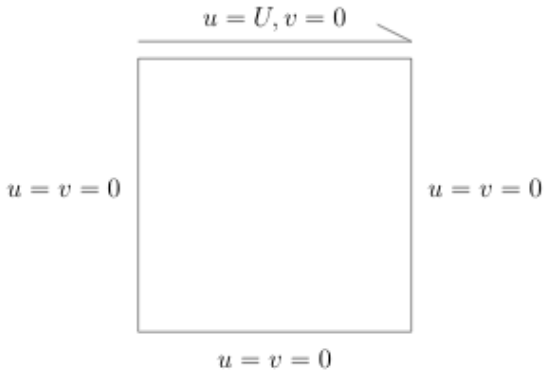

Figure 34: Description of Lid-Driven Cavity problem[14]

The problem is studied considering an unitary height, length and velocity. The Reynolds number is an input, since it determines the performance of the fluid.

4.2.2 Results

In order to verify the code, the results are compared with solutions extracted from literature[15], which are shown in tables 8 and 9. The main code uses QUICK scheme, although it is compared with SMART scheme and UDS. However, results with QUICK are analysed for Reynolds below 5,000, since for highers values the flow becomes turbulent and it is difficult to achieve a steady solution.

	Re						
y	**100**	**400**	**1,000**	**3,200**	**5,000**	**7,500**	**10,000**
0.00000	0.00000	0.00000	0.00000	0.00000	0.00000	0.00000	0.00000
0.05470	-0.03717	-0.08186	-0.18109	-0.32407	-0.41165	-0.43154	-0.42735
0.06250	-0.04192	-0.09266	-0.20196	-0.35344	-0.42901	-0.43590	-0.42537
0.07030	-0.04775	-0.10338	-0.22220	-0.37827	-0.43643	-0.43025	-0.41657
0.10160	-0.06434	-0.14612	-0.29730	-0.41933	-0.40435	-0.38324	-0.38000
0.17190	-0.10150	-0.24299	-0.38289	-0.34323	-0.33050	-0.32393	-0.32709
0.28130	-0.15662	-0.32726	-0.27805	-0.24427	-0.22855	-0.23176	-0.23186
0.45310	-0.21090	-0.17119	-0.10648	-0.08664	-0.07404	-0.07503	-0.07540
0.50000	-0.20581	-0.11477	-0.06080	-0.04272	-0.03039	-0.03800	0.03111
0.61720	-0.13641	0.02135	0.05702	0.07156	0.08183	0.09342	0.08344
0.73440	0.00332	0.16256	0.18719	0.19791	0.20087	0.20591	0.20673
0.85160	0.23151	0.29093	0.33304	0.34682	0.33556	0.34228	0.34635
0.95310	0.68717	0.55892	0.46604	0.46101	0.46036	0.47167	0.47804
0.96090	0.73722	0.61756	0.51117	0.46547	0.45992	0.47323	0.4807
0.96880	0.78871	0.68439	0.57492	0.48296	0.4612	0.47048	0.47783
0.97660	0.84123	0.75837	0.65928	0.53236	0.48223	0.47244	0.47221
1.00000	1.00000	1.00000	1.00000	1.00000	1.00000	1.00000	1.00000

Table 8: 'u' in the vertical center line

	Re						
x	**100**	**400**	**1,000**	**3,200**	**5,000**	**7,500**	**10,000**
0.00000	0.00000	0.00000	0.00000	0.00000	0.00000	0.00000	0.00000
0.06250	0.09233	0.18360	0.27485	0.39560	0.42447	0.43979	0.43983
0.07030	0.10091	0.19713	0.29012	0.40917	0.43329	0.44030	0.43733
0.07810	0.10890	0.20920	0.30353	0.41906	0.43648	0.43564	0.43124
0.09380	0.12317	0.22965	0.32627	0.42768	0.42951	0.41824	0.41487
0.15630	0.16077	0.28124	0.37095	0.37119	0.35368	0.35060	0.35070
0.22660	0.17507	0.30203	0.33075	0.29030	0.28066	0.28117	0.28003
0.23440	0.17527	0.30174	0.32235	0.28188	0.27280	0.27348	0.27224
0.50000	0.05454	0.05180	0.02526	0.00999	0.00945	0.00824	0.00831
0.80470	-0.24533	-0.38598	-0.31966	-0.31184	-0.30018	-0.30448	-0.30719
0.85940	-0.22778	-0.44993	-0.42665	-0.37401	-0.36214	-0.36213	-0.36737
0.90630	-0.16914	-0.23827	-0.51550	-0.44307	-0.41442	-0.41050	-0.41496
0.94530	-0.10313	-0.22847	-0.39188	-0.54053	-0.52876	-0.48590	-0.45863
0.95310	-0.08864	-0.19254	-0.33714	-0.52357	-0.55408	-0.52347	-0.49099
0.96090	-0.07391	-0.15663	-0.27669	-0.47425	-0.55069	-0.55216	-0.52987
0.96880	-0.05906	-0.12146	-0.21388	-0.39017	-0.49774	-0.53858	-0.54302
1.00000	0.00000	0.00000	0.00000	0.00000	0.00000	0.00000	0.00000

Table 9: 'v' in the horizontal center line

4.2.2.1 Mesh study

The study of the mesh size is done in order to analyse its influence on the results, and comparing the evolution of this influence with the Reynolds number.

The first part of the mesh study consists in comparing the solution from tables 8 and 9 with the results obtained through different meshes. This comparison is illustrated in figure 36, where is shown the component 'x' of the velocity along the vertical center line and the component 'y' along the horizontal center line. It is important to realize that the points given in tables 8 and 9 are not enough to achieve a good shape in the graph, so the importance is to coincide with these points.

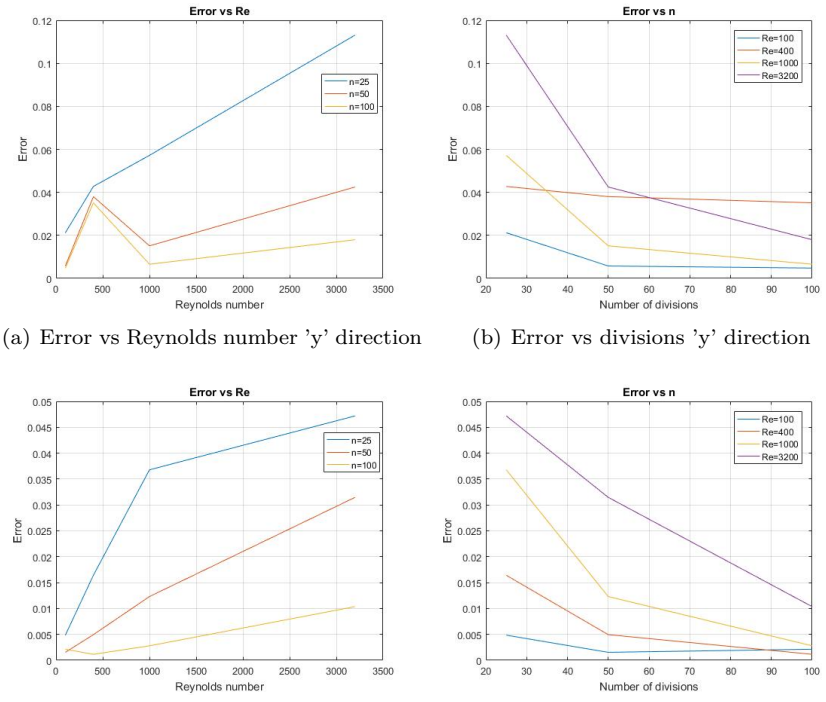

(a) Error vs Reynolds number 'y' direction (b) Error vs divisions 'y' direction

(c) Error vs Reynolds number 'x' direction (d) Error vs divisions 'x' direction

Figure 35: Lid-Driven Cavity values comparison with given solution

Figure 35 represents the error of both velocities (u in figures 35(c) and 35(d), and v in figures 35(a) and 35(b)) in regards to the solution given in tables 8 and 9. As it has been said, the solution is given only in determined points, so it is necessary to do an interpolation in order to get an approximation of the velocity values at the determined coordinates of the solution, enabling to compare the velocities.

Figure 35(a) shows the error between the vertical velocities in the horizontal central line. Although there is a peak in Re=400, it seems to increase the error when increasing the Reynolds number. It makes sense, since the flow becomes more turbulent and it is more difficult to achieve a steady solution. It is also possible to observe that increasing the number of elements decreases the error, that is what is expected. It is also shown in figure 35(b), where the errors for all Reynolds number decrease with the number of divisions. In fact, both graphs are the same expressed in a different way. Moreover, figure 35(b) shows again that there is something that increases the error when Re=400. Graph 36(d) represents the values that give this error, and it is possible to observe that there is a point which seems to be wrong, and it may generate this extra error that changes the expected shape of the graph.

Anyway, figures 35(c) and 35(d) have this expected shape, where increasing the Reynolds num-

ber increases the error in all the meshes, and increasing the number of elements decreases the error with any Reynolds number.

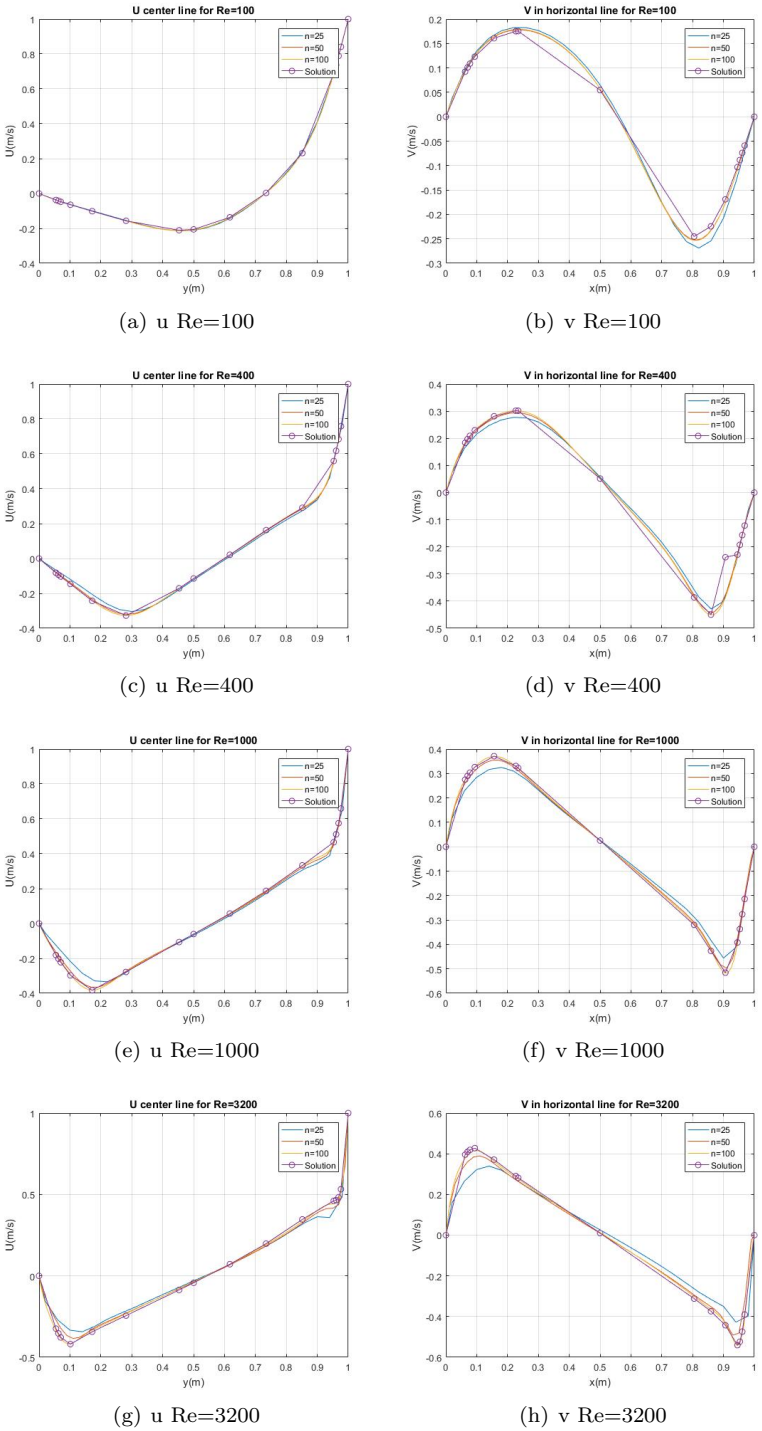

(a) u Re=100 (b) v Re=100

(c) u Re=400 (d) v Re=400

(e) u Re=1000 (f) v Re=1000

(g) u Re=3200 (h) v Re=3200

Figure 36: Lid-Driven Cavity results for different Reynolds

4.2.2.2 Final results

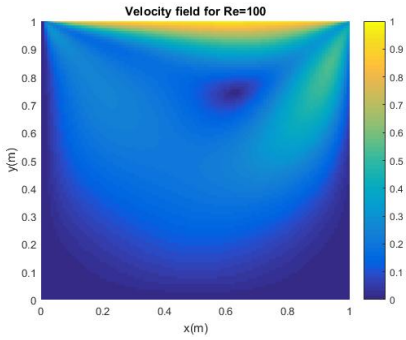

(a) Colormap Re=100

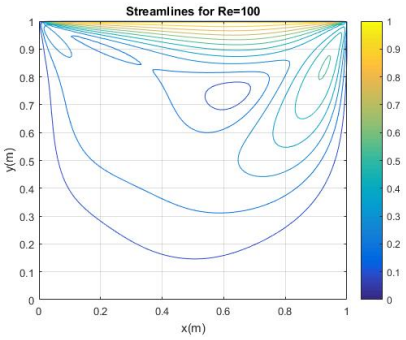

(b) Streamlines Re=100

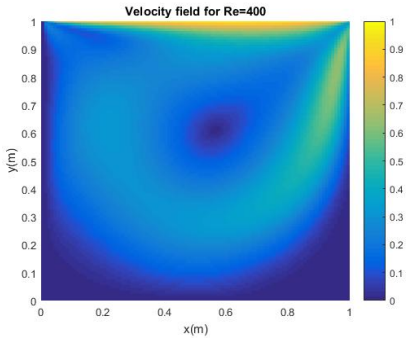

(c) Colormap Re=400

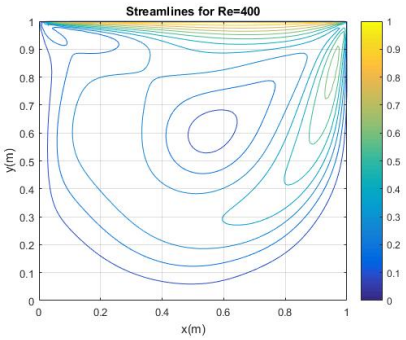

(d) Streamlines Re=400

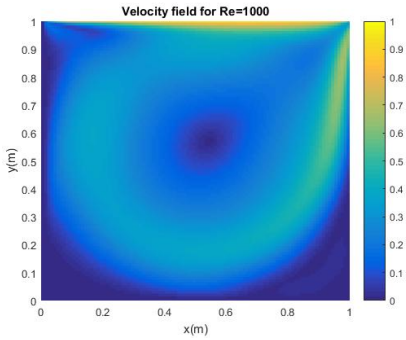

(e) Colormap Re=1000

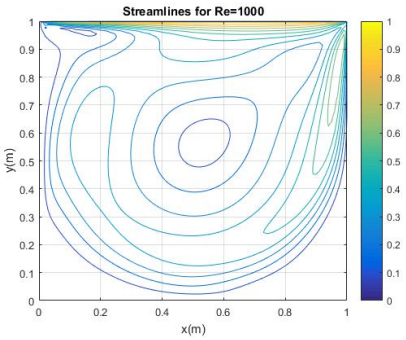

(f) Streamlines Re=1000

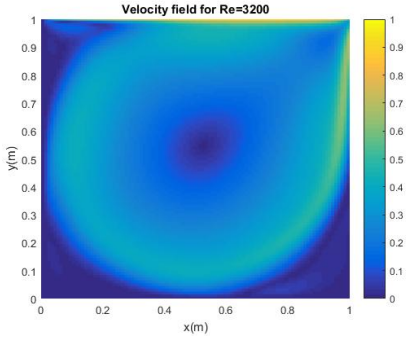

(g) Colormap Re=3200

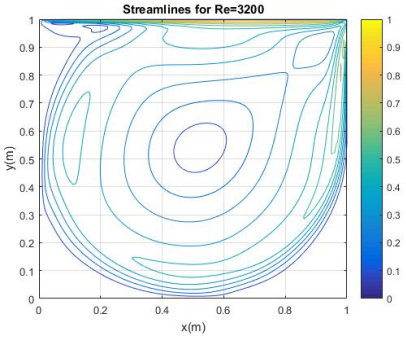

(h) Streamlines Re=3200

Figure 37: Representative resluts Lid-Driven Cavity

4.2.2.3 UDS, QUICK and SMART comparison at high Reynolds number

The aim of this section is to compare the differences between these three schemes at Reynolds highers than 5,000. It is known that from this value, the flow starts to become turbulent and it can be difficult to achieve a steady solution.

As it has been said, QUICK and SMART are high order schemes while UDS is a first order scheme. Figure 38 shows that UDS with a 100x100 mesh gives a solution which is far from the real one, while SMART and QUICK are more accurate.

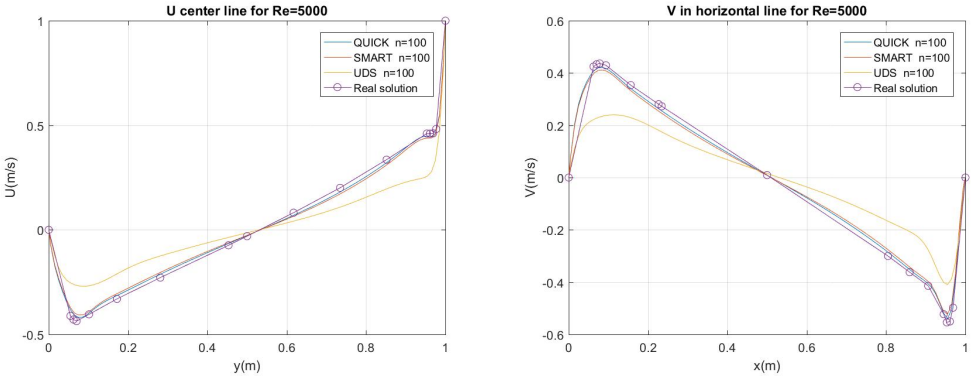

(a) Horizontal velocity (b) Vertical velocity

Figure 38: Comparison between different schemes at Re=5,000 and 100x100 mesh

Figure 39 shows the error and time of computing for the different schemes comparing with the solution given in tables 8 and 9. Obviously, higher the order of the scheme higher the time needed to achieve a solution, but the error decreases considerably.

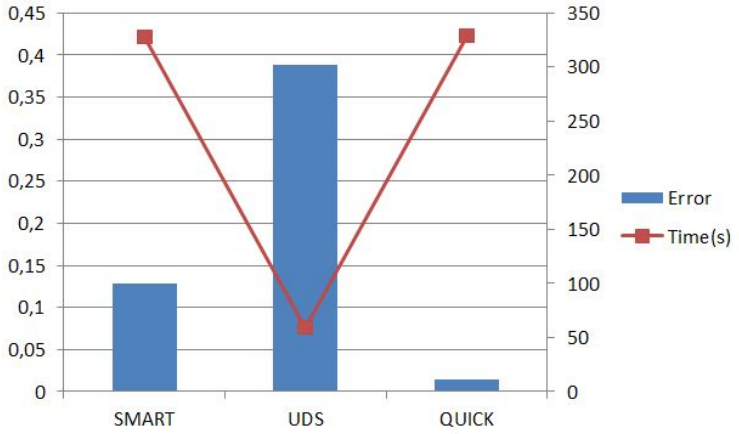

Figure 39: Error comparison with a 100x100 mesh at Re=5,000

Although the minimum error is achieved with QUICK, it is the one which has more difficulties when increasing the Reynolds number. In fact, at Reynolds 10,000 it does not achieve a steady solution. In order to get some values in this regime, an average of the velocities is done through 10,000 time steps. Obviously, and as it can be seen in figure 40, the solution got has a higher error than before. However, it is good enough considering that the values are an average of the unsteady solution.

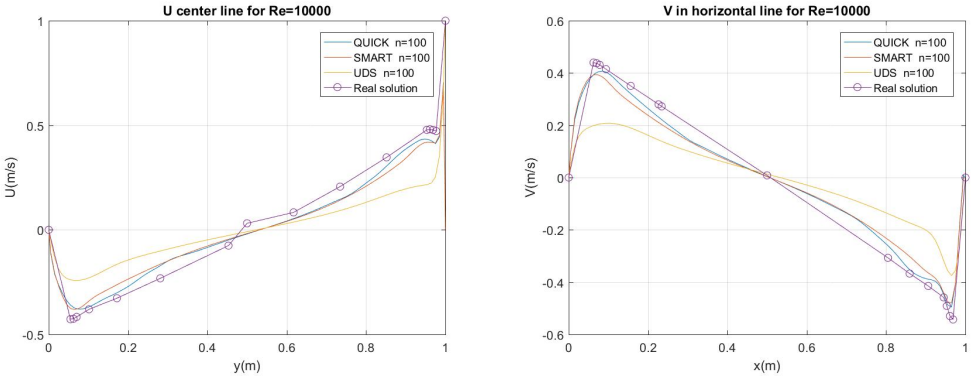

(a) Horizontal velocity (b) Vertical velocity

Figure 40: Comparison between different schemes at Re=10,000 and 100x100 mesh

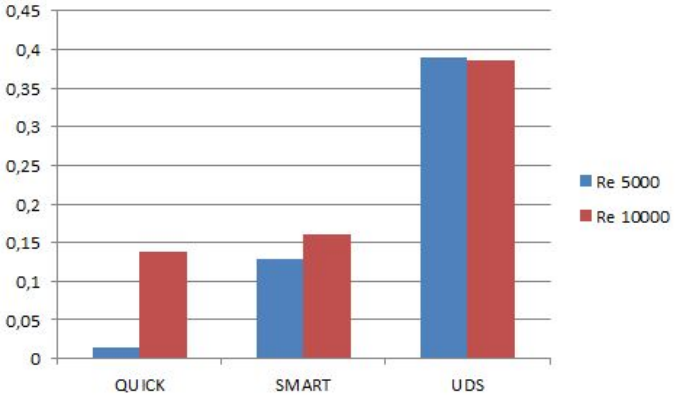

Figure 41: Error comparison with a 100x100 mesh at Re=10,000

4.3 Flow between flat plates

Once Navier-Stokes has been solved and checked with the problem 'Lid-Driven Cavity', the next step is to apply the same code to a different useful applications. The aim is to achieve somehow to simulate a flow tunnel in a laminar regime.

First of all, a laminar flow between two flat plates is simulated , whose analytical solution is known. The pressure loss is found through the Darcy-Weisbach equation [16] (equation 61). In a laminar flow, the friction factor 'f' is inversely proportional to the number of Reynolds, as it is shown in equation 61. However, when the flow becomes turbulent, this factor depends on the surface's roughness as well[17].

$$h_f = f \cdot \frac{L}{D_h} \cdot \frac{V^2}{2g} \qquad \xrightarrow{\text{where}} f = \frac{64}{Re} \tag{61}$$

Equation 61 gives the pressure loss in height of flow units, so it is necessary to multiply by the density of the flow and the gravity. It is important to realize that D_h refers to the hydraulic diameter, which is 4 times the section area divided by the perimeter. As the flow considered is 2D:

$$D_h = 4\frac{WH}{2W + 2H} \xrightarrow{W>>H} D_h = 2H \tag{62}$$

Then, the laminar flow through a pipe is called Poiseuille flow[18].

$$\text{continuity: } \frac{\partial U}{\partial x} + \frac{\partial V}{\partial y} = 0 \quad \xrightarrow{\text{where}} \quad \frac{\partial V}{\partial y} = 0 \quad \xrightarrow{\text{then}} \quad \frac{\partial U}{\partial x} = 0 \tag{63}$$

$$\rho\left(\frac{\partial U}{\partial t}+U\frac{\partial U}{\partial x}+V\frac{\partial U}{\partial y}\right)=-\frac{\partial p}{\partial x}+\mu\left(\frac{\partial^2 U}{\partial x^2}+\frac{\partial^2 U}{\partial y^2}\right) \tag{64}$$

$$\frac{\partial p}{\partial x}=\mu\frac{\partial^2 U}{\partial y^2}=\frac{\Delta p}{L} \tag{65}$$

Integrating equation 65 and establishing the boundary conditions ($U|_{y=H/2}= U|_{y=-H/2}= 0$), equation 66 is achieved.

$$U(y)=\frac{\Delta p}{2\mu L}\left[\left(\frac{H}{2}\right)^2-y^2\right] \tag{66}$$

In order to check the code, the inlet velocities are set. The maximum velocity obtained is substituted in equation 61 to figure out if the pressure difference is the same that the one obtained. Then, this value is used in equation 66 enabling to compare the shape of the velocities profile.

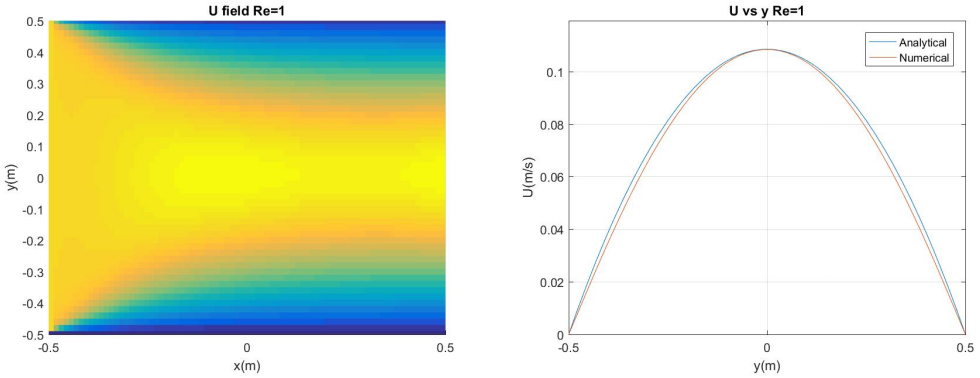

(a) U field

(b) U in a section (numeric vs analytic)

Figure 42: Velocities in 'x' direction between flat plates in laminar flow

Using equation 61, the resultant difference of pressure is $\Delta p = 1.88Pa$. However, as the flow simulated has a constant velocity along the 'y' axis, the pressure at the inlet varies since the flow has to get the expected performance. In fact, the flow starts to feel the effects of the viscosity due to the walls.

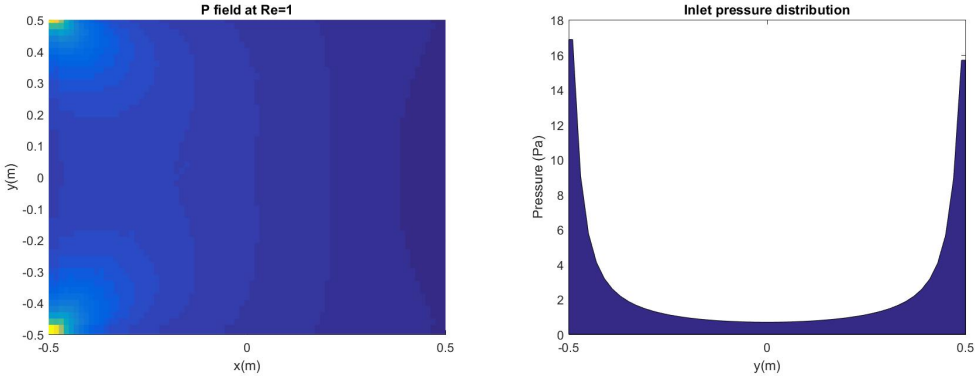

(a) p field

(b) p inlet

Figure 43: Pressure distribution between flat plates

$$\bar{p}=\frac{\int_{-H/2}^{H/2} p\,dy}{\int_{-H/2}^{H/2} dy}=2.47Pa \tag{67}$$

The value of pressure given by equation 61 is p=1.88Pa. Comparing with the value obtained numerically with equation 67 it can be observed that is lower. It makes sense, since equation 61 does not consider that the flow has to be adapted (it does not take into account that the flow is entering with a constant profile of velocities).

4.4 Square Cylinder

4.4.1 Description of the problem

The original square cylinder problem is described in figure 44(a)[19]. However, this section takes into account another possibility, where the walls are moving with a constant velocity (see figure 44(b)). Then, different results are compared between them and also with literature[19].

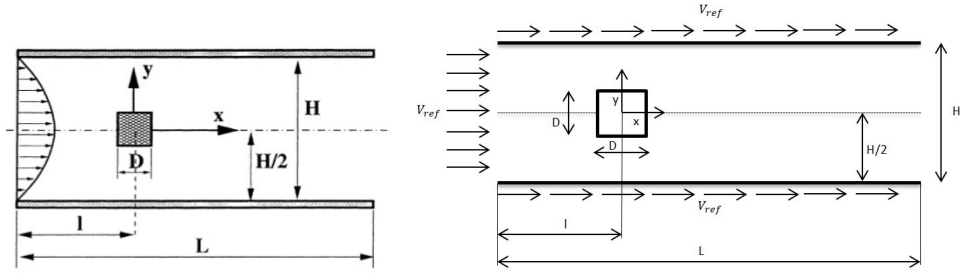

(a) Geometry square cylinder problem[19]

(b) Square cylinder adapted problem

Figure 44: Square cylinder representation

The characteristic length in the Reynolds number is the square cylinder chord, since it allows to compare the results to the literature. Then, the geometry established is shown in table 10.

L(m)	30	**l(m)**	10	**H(m)**	8	**D(m)**	1

Table 10: Geometry values of square cylinder problem

4.4.2 Blocking-off method

The method consists in assigning an infinite viscosity to the solid part of the mesh. Then, it is necessary to make an harmonic mean in order to figure out the viscosity at the cell faces.

$$\mu_e = \frac{d_{PE}}{\frac{d_{Pe}}{\mu_P} + \frac{d_{eE}}{\mu_E}} \tag{68}$$

The procedure followed consists in assigning a viscosity to each node. These values are used to achieve the viscosity at the cell face through equation 68 when 'R' is calculated (equation 55). When the cell face coincides with the square, one of the values of μ is $10^{30} Pa \cdot s$ in equation 68. Then, the fraction of the denominator whose μ is $10^{30} Pa \cdot s$ tends to zero, and disappear from the equation, resulting with expression 69.

$$\mu = \frac{d_{PE}}{d_{Pe}} \mu_P \tag{69}$$

If this value is substituted in Newton's viscosity law (equation 70), the final equation considers the variation of the velocity from the main node to the cell face (where the velocity must be 0).

$$\tau = \mu \frac{\Delta U}{\Delta y} = \frac{d_{PE}}{d_{Pe}} \mu_P \frac{\Delta U}{d_{PE}} \tag{70}$$

Blocking-off method seems to be an easy way to work with solid bodies, since the only task needed is to assign the correct viscosity to each node. However, this method generates several problems when the flow becomes turbulent, and the mesh density needed increases with the complexity of the geometry. In fact, as it has been said before, the roughness of a surface is important in a turbulent flow, and it is difficult to simulate with this method in a complex geometry. Anyway, turbulent flow is not studied in this thesis.

4.4.3 Mesh discretization and boundary conditions

As it can be seen in figure 45, the resultant grid is non-equidistant. There are two main reasons to use this kind of mesh:

- It allows to accurate differently the parts of the problem, since there are zones which requires more precision.
- Because of the staggered meshes and the blocking-off method, it is necessary to have cell faces at the walls of the square cylinder.

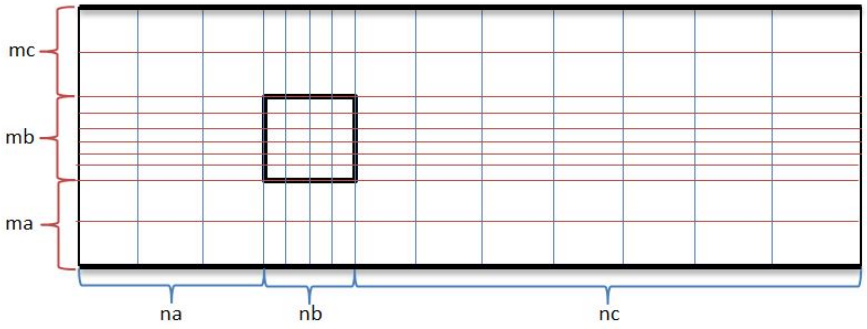

Figure 45: Mesh used with the square cylinder

Complexity of mesh generation increases due to the necessity of split in parts the main and the staggered meshes. Figure 46 represents a real mesh generated by the code used, and it is possible to see that the grid density is different depending on the zone.

The boundary conditions for the pressure computation are that the derivative at each wall must be 0 (including the inlet and the outlet). However, the important issue is the velocity boundary conditions. At the inlet, the velocity field is imposed (parabolic or constant velocities, depending on the case), and at the outlet the velocity derivative must be 0. This boundary condition is important because if the velocity is imposed in the outlet it would affect the wake of the flow.

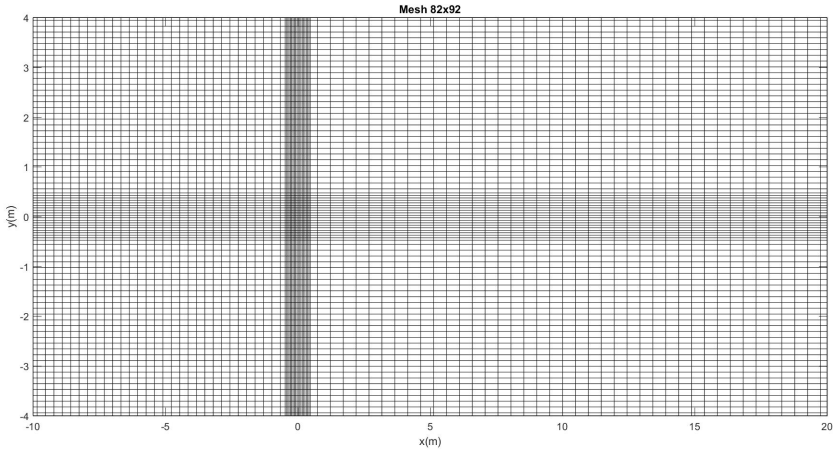

Figure 46: Mesh generated with na=30 nb=20 nc=40 and ma=30 mb=20 mc=30

4.4.4 Results Re=1

Figure 47 shows the streamlines for both cases mentioned: when walls are moving with a constant velocity and when they are static. At this Reynolds number the results are very similar talking about the streamlines. It is important to remind that in the static walls case the velocity profile at the inlet is parabolic while the moving walls case is a constant profile.

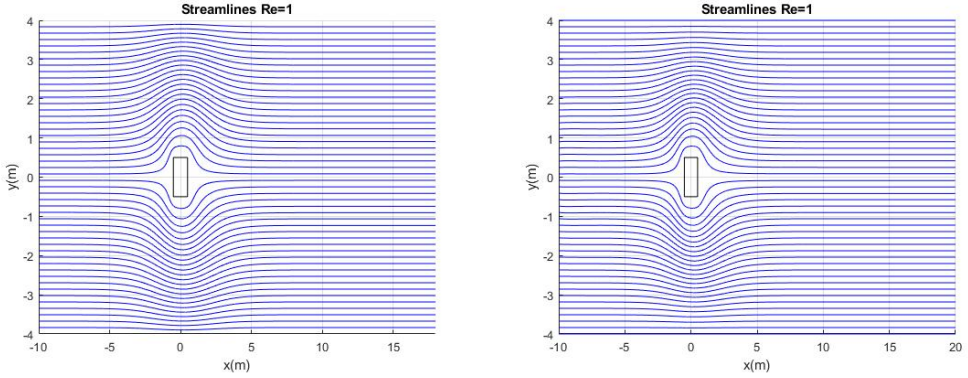

(a) Static walls

(b) Walls moving at Vref

Figure 47: Streamlines around square cylinder Re=1

In figure 48 are shown the 'x' components of the velocities along the center line (y=0m) for both cases. Again, both cases are very similar, and there is no a representative difference between them.

Then, figure 49 represents the velocities profiles at different x coordinates. The first graph in figure 49(a) represents the 'x' component of the velocity. When x=0 (middle of the square cylinder), it has a parabolic shape at both sides of the square. It would be like a Poiseuille flow shown in section 4.3. Then, behind the cylinder (x=4D) the velocity is recovering the initial values. If figure 48 is taken into account, it makes sense that increasing the distance from the square increases the maximum velocity value at y=0m.

Then, talking about the 'y' components of the velocity, above the square cylinder are positive and below are negative, although behind the square cylinder they change their sign. This is what

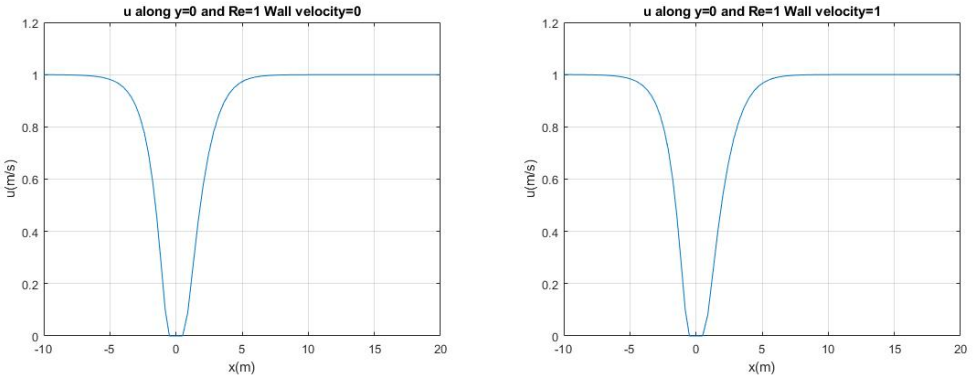

(a) Static walls (b) Moving walls

Figure 48: Velocities profile square cylinder at y=0 and Re=1

is expected, since before pass through the cylinder the flow which is going up pass over the square, and then it must go down again, and the same happens below.

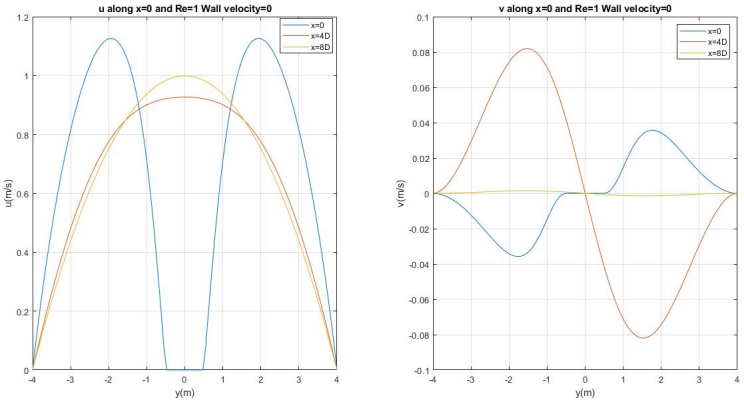

(a) Static walls

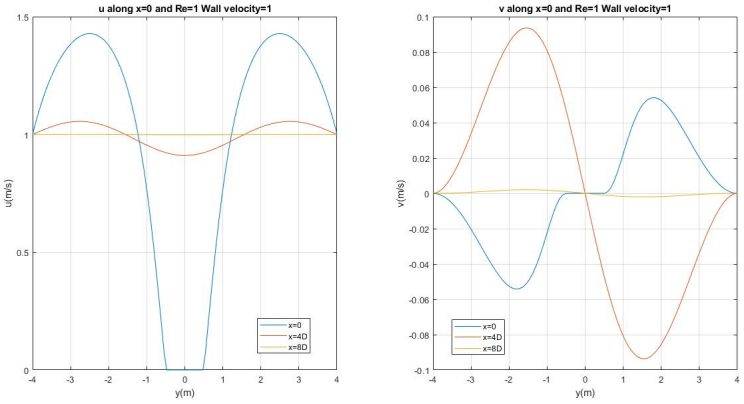

(b) Moving walls

Figure 49: Velocities profile square cylinder at different x positions and Re=1

The 'y' components of figure 49(b) are very similar to the other case, so the performance in this

direction remains equal. However, the velocities in the 'x' direction are quite different. The flow at x=0 is a mixture of Poiseuille and Couette [20], where the second one considers that one of the walls is moving with constant velocity. The shape is parabolic too, but not centered. Moreover, the maximum velocity is higher than the reference one ($V_{ref} = 1m/s$) since it is performing as a nozzle. Finally, the velocity at y=0m behind the square recovers its initial value, as it has been shown in figure 48(b).

4.4.5 Results Re=30

In figure 50 it is possible to see that when the Reynolds number is increased appears vorticity behind the square. It can be observed that both cases are very similar in this regime too.

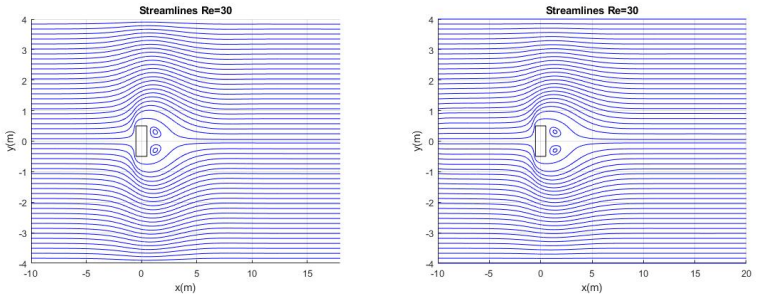

(a) Static walls (b) Walls moving at Vref

Figure 50: Streamlines around square cylinder Re=30

Now exists a negative velocity in the 'x' direction behind the square (see figures 51(a) and 51(b)). It makes sense with figure 50, since the vorticity generated behind the square implies a zone of negatives velocities.

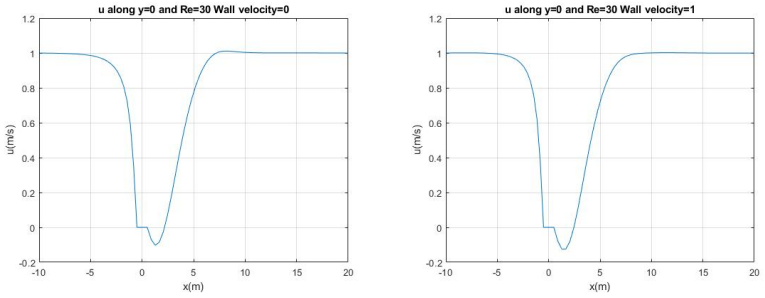

(a) Static walls (b) Moving walls

Figure 51: Velocities profile square cylinder at y=0 and Re=30

Talking about the velocities profiles at different 'x' sections, the 'x' component of the velocity loses the parabolic profile in both cases. It is still accelerated when passes above and below the square, but there is no Poisseuille flow. The 'y' components are very similar, but their values are increased comparing with Re=1. Moreover, at x=0m, the slope of the velocity change in the 'y' direction at the square cylinder walls is higher compared to Re=1.

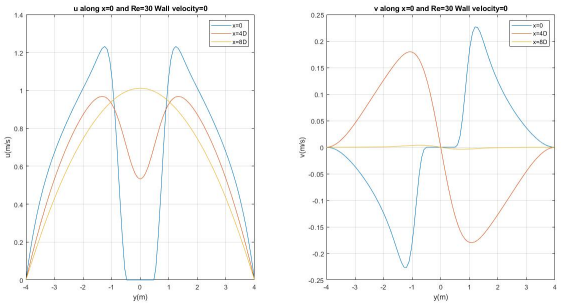

(a) Static walls

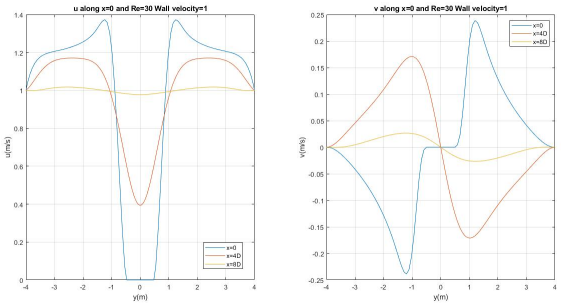

(b) Moving walls

Figure 52: Velocities profile square cylinder at different x positions and Re=30

4.4.6 Drag coefficient

Drag coefficient is found for different Reynolds which solutions are steady flows. In order to get this coefficient, pressure is evaluated behind and in front of the square cylinder through equation 67. Once it is done, it is possible to calculate the force that the square is doing to the fluid multiplying the pressure difference by the height of the section. However, it is still necessary to take into account the viscous stresses. To get these values, it is necessary to apply the Newton's law shown in equation 71, where the stress is the product between the viscosity and the velocity gradient. In fact, it is a simplification of equation 2k.

$$\tau = \mu \frac{\partial u_i}{\partial x_i} \tag{71}$$

However, τ has units of pressure, so it has to be multiplied by the differential areas.

Once it is done, drag coefficient is achieved dividing the resultant force due to viscosity and pressure by the dynamic pressure multiplied by the cylinder square chord.

Figure 53 shows the evolution of the drag in front of the Reynolds number. Both cases presents good results comparing with literature (figure 53(a)), decreasing the drag when the Reynolds number is increased.

The moving walls case seems to have more drag at highers Reynolds numbers. It can be explained considering that the average velocity field is higher than the static walls case, although it is divided by the same dynamic pressure. In other words, the static wall case would have to be divided by a lower velocity, since the average is not the same as the moving wall case.

In figure 54 it can be observed the contribution of each force to the total drag. It is known

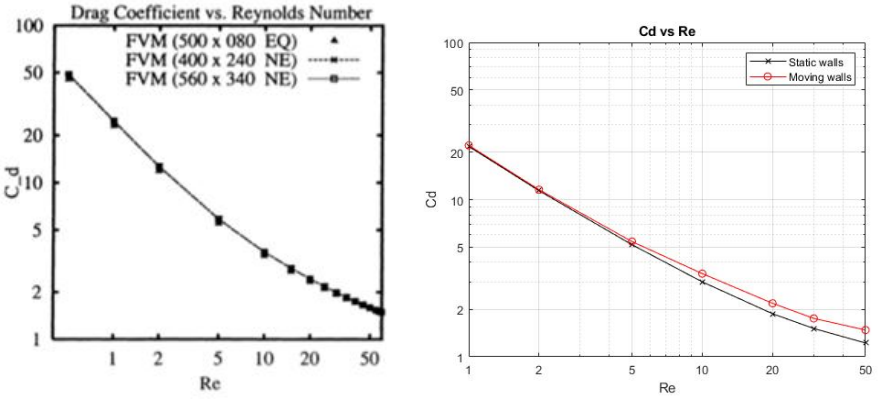

(a) Drag coefficient literature[19]

(b) Results drag coefficient

Figure 53: Drag coefficient vs Reynolds square cylinder

that the Reynolds number quantifies the importance of the viscous forces in front of the inertial forces, and that highers Reynolds numbers mean less viscous forces. This is the performance in both cases, decreasing the viscosity importance when the Reynolds number is increased. However, the viscosity in the moving walls case has less contribution to the total drag. As it has been said, the average velocity field is higher in the moving walls case, and it performs as if its Reynolds were higher.

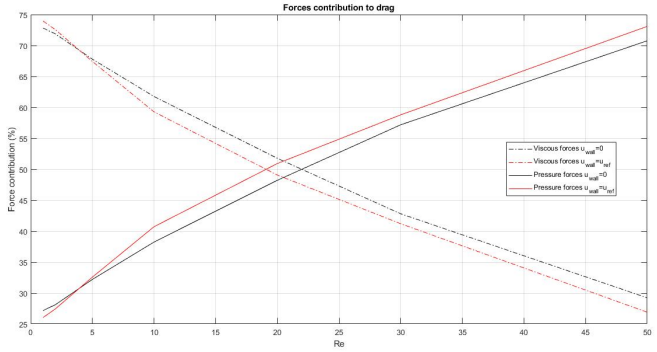

Figure 54: Forces contribution to drag

4.4.7 Results Re=100

At this Reynolds number the flow is unsteady. In order to get some results, it is got the same criteria as the literature[19]. It consists in stop the code when the 'y' velocity at x=10D changes its sign.

First of all, results from literature are shown in order to compare them. Graphs from figures 55 and 56 are results from two different methods: FVM and LBA. Both are very similar, but the interesting one to compare with the results of this thesis are FVM (Finite Volume Method).

It is important to say that the results of figures 55 and 56 are got with a high accurate mesh which can not be computed with these thesis resources. Therefore, results shown since now are less accurate than the ones from literature.

Since now, and in order to study deeply the difference between the results, both cases are studied separately.

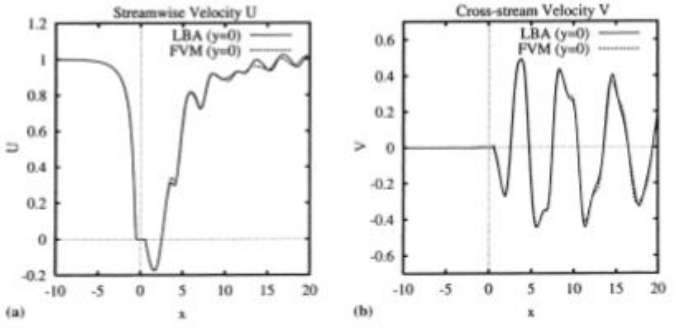

Figure 55: Square cylinder velocities along y=0m[19]

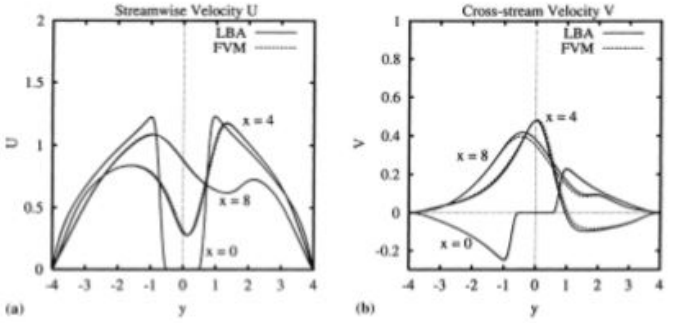

Figure 56: Square cylinder velocities along different 'x' sections[19]

4.4.7.1 Static walls

Figure 57(a) shows the magnitude of the velocity in the 'x' direction, while figure 57(b) shows the streamlines. There is vorticity behind the square cylinder, but the symmetry which has characterized the flow until now is lost and, moreover, the wake affects the flow from the square to the outlet.

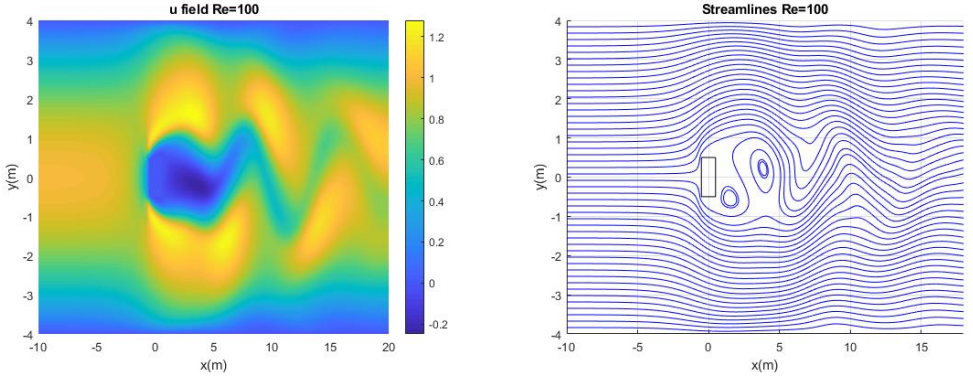

(a) u field (b) Streamlines

Figure 57: Static walls velocity and streamlines for Re=100

Behind the square there are again negative velocities in the 'x' direction (see figure 58), but the velocity has some disturbances generated by the wake. The vertical components of the velocity

change their sign along y=0, creating the sinusoidal shape of figure 57(b) behind the square. Both graphs have a shape similar to the literature (figure 55), but as it has been said, they are less accurate.

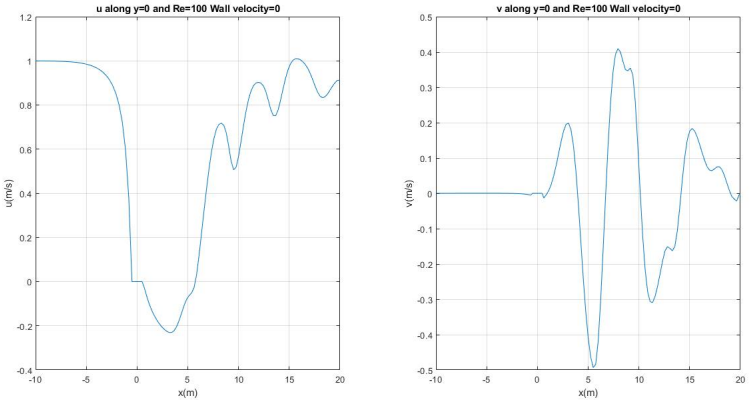

Figure 58: 'x' velocity at y=0 for Re=100

Since the symmetry behind the square cylinder is lost, both components of velocity have different profiles depending on the 'x' position and the time (see figures 59). It is important to realize that the results presented until now (for Reynolds 100) are for a singular moment of time, as an instantaneous picture. Actually, there is a time evolution of the wake which is not shown in these figures.

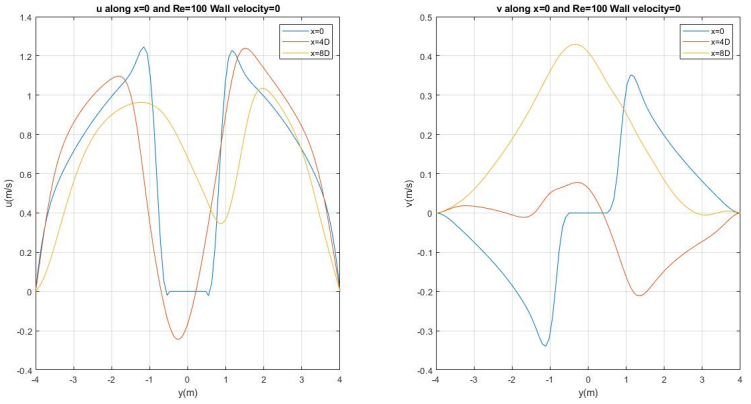

Figure 59: 'y' velocity for different 'x' for Re=100

4.4.7.2 Moving walls

The moving walls case has less freedom than the static walls, since the wake is impulsed by both walls (figure 60). The streamlines behind the body seems to have a more organized sinusoidal shape and less vorticity comparing with figure 57(b).

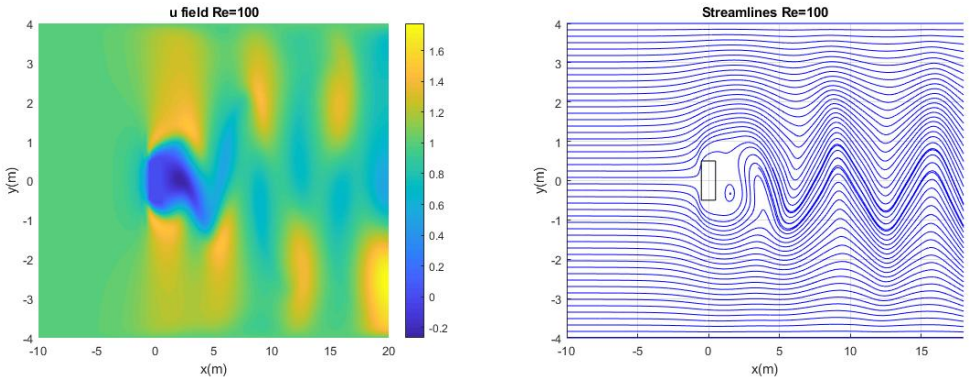

(a) u field (b) Streamlines

Figure 60: Moving walls velocity and streamlines for Re=100

The vertical velocity behind the square cylinder seems to follow a periodic shape, with positives and negatives velocities at both sides of the center. In fact, it is similar to the static walls case, but again seems more organized. Comparing the results to literature (figure 55), moving walls case is more similar talking about the vertical components, and static walls case talking about the horizontal components.

The horizontal component of the velocity in the moving walls case decreases near the outlet. It is known that the mass must be conserved, so the same flow which enters through the inlet must exit through the outlet. Figure 60(a) shows that the horizontal component of the velocity in the outlet is increased between y=-1m and y=-4m. It justifies that the other velocities in the outlet must equilibrate the mass flow reducing their values.

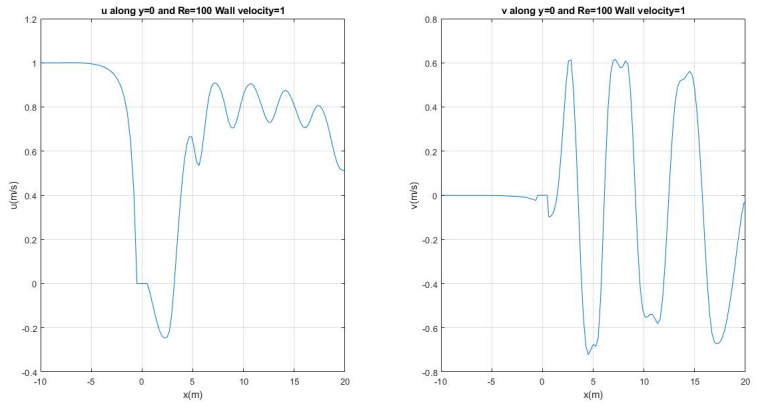

Figure 61: 'x' velocity at y=0 for Re=100

Velocities of figure 62 behind the square are asymmetric, and their performance is similar to the static walls case and literature (despite the fact that the velocity at the walls is 1m/s).

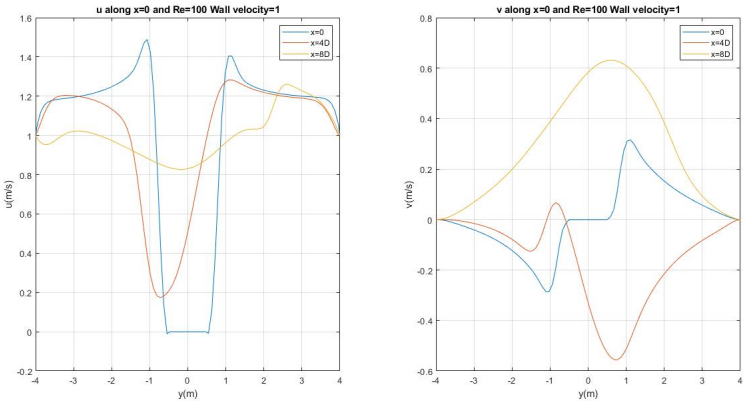

Figure 62: 'y' velocity for different 'x' for Re=100

4.5 Rhombus

An interesting geometry to study is a rhombus with different slenderness ratios ('a' from equation 72).

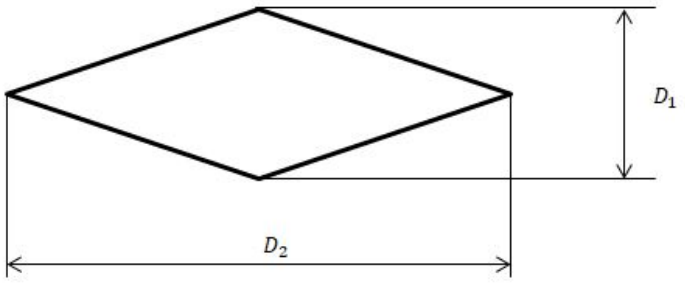

Figure 63: Rhombus geometry definition

$$a = \frac{D_2}{D_1} \tag{72}$$

It is known that higher slenderness provides better aerodynamic performance. However, at low Reynolds number, it is not true at all. In this regime, viscous and pressure forces are the same order of magnitude, and increasing the slenderness means increasing the surface forces. In fact, the pressure forces are not as important since the Reynolds number is too low and there is no detachment of the flow from the surface.

In figure 64 are shown the streamlines around the rhombus for two different Reynolds and two different slenderness. When the diagonal ratio is 1, there is vorticity behind the rhombus and, for Re=150, the flow is unsteady. In fact, both results are similar to the square cylinder streamlines for these Reynolds numbers. However, when the diagonal ratio is increased the vorticity disappears.

Higher slenderness provides better aerodynamic performances when the Reynolds number is high, and the viscous stresses lose strength in front the pressure forces. For low Reynolds numbers, as the ones treated in this thesis, increasing the slenderness means reducing the pressure forces but increasing the viscous surface. Therefore, the viscous stresses take importance when the diagonal ratio is increased, while the pressure forces are decreased due to the aerodynamic shape.

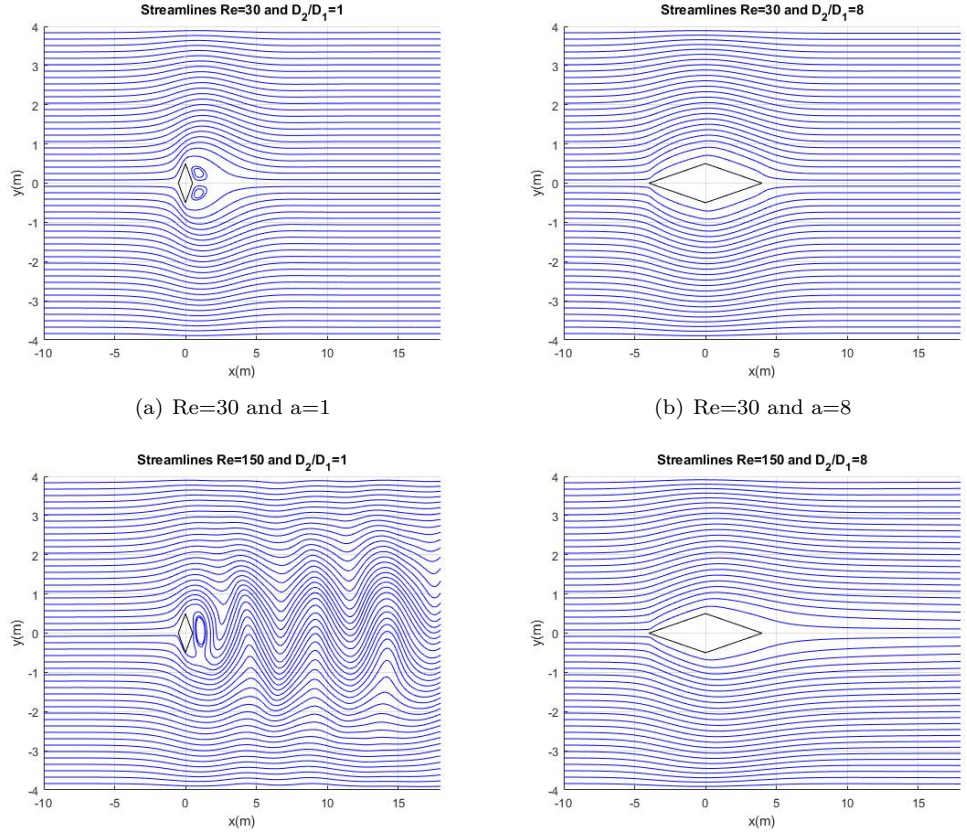

(a) Re=30 and a=1

(b) Re=30 and a=8

(c) Re=150 and a=1

(d) Re=150 and a=8

Figure 64: Different streamlines around rhombus for different Reynolds and slenderness

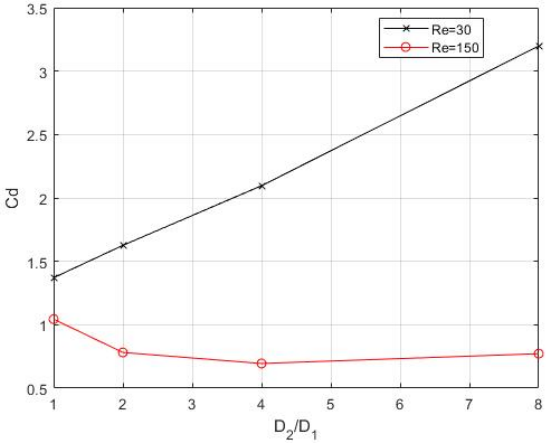

Figure 65: Rhombus drag in front of the slenderness variation for Re=30 and Re=150

Figure 65 shows the drag coefficient in front of the diagonal ratio for two different Reynolds. With Re=30, when the slenderness is increased the drag coefficient increases too. It makes sense, since for low Reynolds numbers the viscosity has more importance, and increasing the surface increases the force. It does not happen when Re=150, because at this Reynolds the viscosity has less importance than the pressure forces.

In picture 66 it is possible to see that when the diagonal ratio is increased (more surface) the

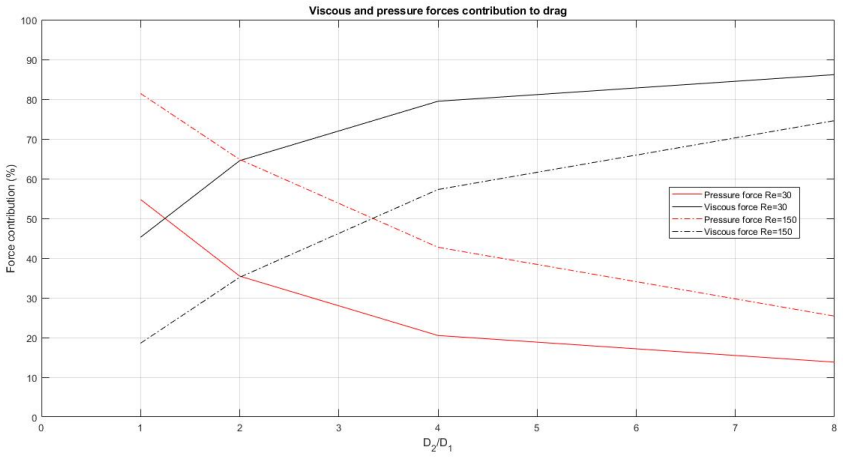

Figure 66: Rhombus forces contribution to drag in front of the slenderness variation for Re=30 and Re=150

viscous stresses take importance to the drag contribution. With Re=30 both forces are the same order of magnitude, increasing the viscous importance when the surface is increased. When Re=150, pressure is the main force for a=1. Then, increasing the slenderness, this pressure loses importance in front of the viscosity, but actually the drag is also reduced (see figure 65). It means that, despite increasing the viscosity contribution to the drag, at this Reynolds number the importance remains in the Pressure forces since the total drag is reduced.

4.6 Circular cylinder

As it has been said, blocking-off method with structured meshes allows to compute different solid geometries which are relatively complex. The only task needed is to assign correctly the nodes of the body with their infinite viscosity. In order to show that, a circular cylinder is computed with its basics results at lows Reynolds numbers.

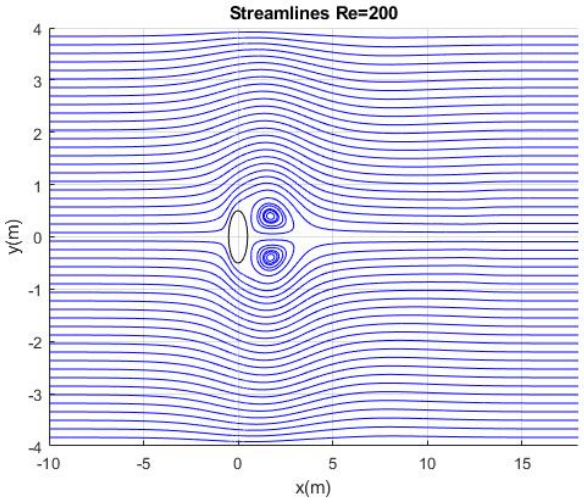

Figure 67: Streamlines around circular cylinder at Reynolds 200

As it is shown in figure 67, the performance of the flow around the circular cylinder at Reynolds

200 is similar to the one obtained with the square cylinder at Reynolds 30. It is a basic proof that the circular shape is less disturbing than the square.

4.7 NACA 0016 and future improvements

NACA airfoils are used mainly to study the aerodynamic performance of the air around a wing section. These kind of airfoils are easily defined with mathematical expressions, and the easiest ones are the 4 digits NACA (mpXX)[21]. The first one specifies the maximum camber (m) in percentage of chord. The second one (p) shows where is located the maximum camber in tenths of chord. The last 2 digits express the maximum thickness in percentage of chord.

The camber of the airfoil is defined by equations 73a and 73b, and the extrados and intrados are expressed through equation 73c, which represents a relative position from the camber.

$$y_c = \frac{m}{p^2}(2px - x^2) \qquad \text{from x=0 to x=p} \tag{73a}$$

$$y_c = \frac{m}{(1-p)^2}((1-2p) + 2px - x^2) \qquad \text{from x=p to x=D} \tag{73b}$$

$$\pm\, y_t = \frac{t}{2}(0.2969\sqrt{2} - 0.1260x - 0.3516x^2 + 0.2843x^3 - 0.1015x^4) \tag{73c}$$

This thesis shows the streamlines for a symmetric airfoil (0016) in a laminar flow (figure 68), which does not make sense since these kind of airfoils are used at high Reynolds number. When the geometry of the solid body is more complex, blocking-off method with structured meshes is useless for turbulent flows, since it is difficult to analyse correctly the surface roughness (which takes importance when the flow is turbulent).

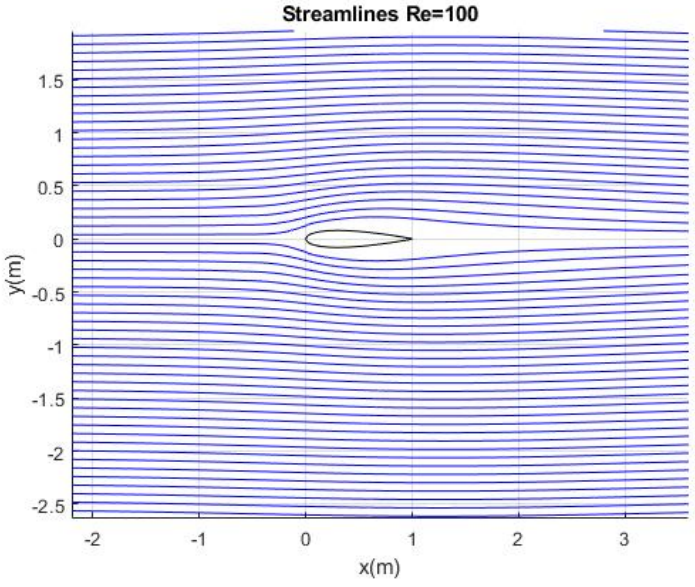

Figure 68: Streamlines around NACA 0016 for Re=100

The next step in this thesis would be the unstructured meshes, enabling the development of complex geometries without the necessity of increasing the mesh density. In this way, it would allow to compute turbulent flows using any method as RANS (Reynolds-averaged Navier-Stokes), DNS (Direct Numerical Simulation) or LES (Large Eddy Simulation) [22]. These methods are used to compute the turbulence of the flow, taken into account the accuracy needed and the computational cost required.

4.8 Conclusions

Fractional Step Method with staggered meshes has been a useful tool to solve the Navier-Stokes equations in laminar flows. As it is said in the thesis, despite its simplicity, it provides good results without high computational cost. However, with the 'Lid-Driven Cavity' has been shown the importance of the convection scheme, and its influence to the results when the Reynolds number is increased.

Blocking-off method has been an easy way to simulate solid geometries inside the domain. In the square cylinder case, it provides good results since the mesh is completely adapted to the geometry. In fact, it would be possible to simulate turbulent flow with these conditions, although the density of the mesh and the accuracy would have to be increased.

The other geometries studied provide good results too, but the mesh density have been increased in order to simulate the most accurate geometry. In this case, turbulent flow would not be possible because the surfaces of the body are not well-defined enough to consider the roughness.

5 Final conclusions

Numeric calculus is a reality which has an important role nowadays, used in most of the engineering fields. Its study implies a continuous combination between the physical and mathematical knowledge with their implementation to computer codes, always looking for the highest efficiency in order to reduce the computational cost. This thesis have studied basic methods, which are an introduction to numerical calculus, in spite of their complexity.

Computational Fluid Dynamics is a particular case of numerical calculus, which has a lot of importance in real applications. It has been worked mainly with the Navier-Stokes equations with incompressible flow, but it is only a small part of what is possible with Computational Fluid Dynamics, as turbulence, compressible flows, supersonic flows... The analyses carried out with this type of simulations allow companies to save a lot of money aimed to experimental research, optimizing the models before building them.

Fractional Step Method is a simple way to solve Navier-Stokes with incompressible flow. As it has been said in this thesis, it is an explicit method and it means that the time step needed is low. Then, it spends more time before a steady solution is got, since it has to solve a lot of time steps. Anyway, it provides good results with relatively simple meshes. Its combination with blocking-off method allows to perform good simulations of complex geometries in laminar flow. However, it is necessary to increase the mesh density when the solid geometry is complex.

Although this thesis has not treated turbulent flows, Fractional Step Method is also useful to do these kind of study. The problem is that the mesh density needed is very high, and the geometries must be well defined since the roughness of the surfaces takes importance.

There would be two ways to carry on this thesis. The first one consists in simulate the turbulence with the same mesh for the square cylinder, since its geometry is absolutely adapted to the mesh. In this way, it could be used any of the turbulent methods mentioned: Direct Numerical Simulations (DNS), Reynolds Averaged Navier Stokes (RANS) or Large Eddy Simulations (LES). RANS is the one which requires less computational cost, and would be the most feasible method.

The other way would be the change to unstructured meshes, and start simulating again laminar flows to check their validity. Once they were solved, the next step would be to work with turbulent flows, where it would be possible to simulate complex geometries with good results.

6 Acknowledgments

Finally, to conclude the thesis, specially thank to heat and transfer technological center CTTC from Universitat Politecnica de Catalunya (UPC) for all the library resources and the help received when in doubt. Giving a special thanks to Professors Asensio Oliva for his leadership in the project, Carles David for the guidance and for all the specific advices given in the computational part as well as in the written one, Xavier Trias for helping in the IT part of the external flow and Jorge Chivas for the advices received and for managing and supporting the introductory part of convention-diffusion.

References

[1] *XFlow CFD - Release 2017*. URL: http://www.xflowcfd.com/xflow2017 (visited on 03/02/2018).

[2] NASA. *Navier Stokes Equations - https://www.grc.nasa.gov/www/k-12/airplane/nseqs.html*.

[3] CMI. *Rules for the Millennium Prizes*. 2012. URL: http://www.claymath.org/millennium-problems/rules-millennium-prizes.

[4] *Notes 'Gas dynamics and heat flow' - Convection mathematical formulation manuscript*.

[5] CTTC - Universitat Politècnica de Catalunya. "A Two-dimensional Transient Conduction Problem". In: (2014), pp. 3–5.

[6] Suhas V. Patankar. *Numerical heat transfer and fluid flow*. 1980. DOI: 10.1002/cite.330530323. URL: http://books.google.fr/books?id=5JMYZMX3OVcC.

[7] Samuel Kotz. "Tridiagonal Matrix". In: 1.2 (2004), pp. 1–5. ISSN: 9780471667193. DOI: 10.1002/0471667196.ess2763.

[8] "Verification strategies for the convection-diffusion equation - from subject analysis of thermal and fluid dynamics issues in industrial and/or aeronautical systems and equipment". In: (), pp. 1–5.

[9] *Convection-diffusion equations - notes from assignment analysis of thermal and fluid dynamics issues in industrial and/or aeronautical systems and equipment*.

[10] M. S. Darwish and F. H. Moukalled. "Normalized variable and space formulation methodology for high-resolution schemes". In: *Numerical Heat Transfer, Part B: Fundamentals* 26.1 (1994), pp. 79–96. ISSN: 15210626. DOI: 10.1080/10407799408914918.

[11] CTTC department. "Numerical Solution of Convection". In: (2012), pp. 1–15.

[12] CTTC. "Introduction to the Fractional Step Method". In: (), pp. 1–10.

[13] CTTC (UPC). "Fractional Step Method Staggered Meshes". In: ().

[14] *Lid-driven cavity problem – CFD-Wiki*. URL: https://www.cfd-online.com/Wiki/Lid-driven_cavity_problem.

[15] U. Ghia, K. N. Ghia, and C. T. Shin. "High-Re solutions for incompressible flow using the Navier-Stokes equations and a multigrid method". In: *Journal of Computational Physics* 48.3 (1982), pp. 387–411. ISSN: 10902716. DOI: 10.1016/0021-9991(82)90058-4. arXiv: arXiv:1011.1669v3.

[16] *DarcyWeisbach equation*. URL: https://en.wikipedia.org/wiki/Darcy-Weisbach%7B%5C_%7Dequation.

[17] Frank White. "Fluid Mechanics". In: *McGraw-Hill,New York* (2010), p. 862. ISSN: 1364-0321. DOI: 10.1111/j.1549-8719.2009.00016.x.Mechanobiology. arXiv: 1003.3921v1.

[18] R Castilla P J Gamez-montero and Ecuaciones De. "Flujo con viscosidad dominante II". In: (2012), pp. 1–4.

[19] M. Breuer et al. "Accurate computations of the laminar flow past a square cylinder based on two different methods: Lattice-Boltzmann and finite-volume". In: *International Journal of Heat and Fluid Flow* 21.2 (2000), pp. 186–196. ISSN: 0142727X. DOI: 10.1016/S0142-727X(99)00081-8.

[20] Bombay. "Principle of Fluid Dynamics Module". In: (2006), pp. 1–72. URL: http://nptel.ac.in/courses/101103004/pdf/mod5.pdf.

[21] En Jacobs, Ke Ward, and Rm Pinkerton. "The characteristics of 78 related airfoil sections from tests in the variable-density wind tunnel". In: *National Advisory Committee for Aeronautics* (1933), pp. 299–354. ISSN: 1098-6596. DOI: 10.1017/CBO9781107415324.004. arXiv: arXiv:1011.1669v3. URL: http://oai.dtic.mil/oai/oai?verb=getRecord%7B%5C&%7DmetadataPrefix=html%7B%5C&%7Didentifier=ADA801175.

[22] UPC CTTC. "Direct Numerical Simulation (DNS), Reynolds Average Navier-Stokes and Large Eddy Simulation (LES) Modelling Regularization". In: ().